Surfaces and Interfaces 97 (2026) 110232

Contents lists available at ScienceDirect

Surfaces and Interfaces

journal homepage: www.sciencedirect.com/journal/surfaces-and-interfaces

Functional CuI–PVA hybrid sol–gel coatings for cotton fabrics: Synthesis, characterization, and antibacterial performance

Valentina Trovato [a,b,1,*], Maria Josè Lo Faro [c,d,1], Giulia Rando [e,*], Maurilio Galletta [f], Agnese D'Agostino [a,b], Serena Facchiano [g], Claudia Vineis [g], Raphael Palucci Rosa [a], Silvia Sfameni [e], Giuseppe Rosace [a,b,2], Maria Rosaria Plutino [e,*,2]

[a] Department of Engineering and Applied Sciences, University of Bergamo, Viale Marconi 5, 24044, Dalmine, BG, Italy
[b] Local CSGI (Inter-University Center for Colloid and Surface Science) Research Unit, 24044, Dalmine, BG, Italy
[c] Department of Physics and Astronomy, University of Catania, Via Santa Sofia 64, 95123, Catania, Italy
[d] Institute for Microelectronics and Microsystems – National Research Council (IMM–CNR), Via Santa Sofia 64, 95123, Catania, Italy
[e] Institute for the Study of Nanostructured Materials – National Research Council (ISMN–CNR), URT Messina, c/o Department of ChiBioFarAm, University of Messina, Viale F. Stagno d'Alcontres 31, Vill. S. Agata, 98166, Messina, Italy
[f] Institute for Microelectronics and Microsystems – National Research Council (IMM–CNR), Messina, c/o Department of ChiBioFarAm, University of Messina, Viale F. Stagno d'Alcontres 31, Vill. S. Agata, 98166, Messina, Italy
[g] Institute of Intelligent Industrial Technologies and Systems for Advanced Manufacturing – National Research Council (STIIMA-CNR), Corso Giuseppe Pella 16, 13900, Biella, Italy

ARTICLE INFO

Keywords:
CuI particles
Sonochemical synthesis
Sol–gel
Antibacterial finishing

ABSTRACT

This work reports the development of a hybrid CuI–PVA/siloxane sol–gel finishing for antibacterial cotton fabrics. CuI particles were synthesized by a sonochemical route, stabilized in poly(vinyl alcohol) (PVA), and incorporated into a GPTMS/TEOS-derived sol–gel matrix. The resulting dispersions, containing 2.04 and 4.08 wt % CuI–PVA, were applied to cotton by a conventional pad–dry–cure process. The CuI–PVA dispersions and the treated fabrics were characterized by FTIR and Raman spectroscopy, SEM-EDS, and washing durability tests. The results indicate the formation of a siloxane network that anchors the CuI–PVA phase onto the cotton surface without compromising the morphology of the substrate. Both formulations exhibited marked antibacterial activity against *Staphylococcus aureus* ATCC 6538 and *Escherichia coli* ATCC 11229, with bacterial reductions higher than 99% under the tested conditions. This antibacterial performance was substantially retained after three ISO 105-C10 washing cycles. Overall, the proposed CuI–PVA/siloxane system represents a simple and scalable proof-of-concept strategy for imparting antibacterial functionality to cotton fabrics intended for hygienic and technical applications.

1. Introduction

Textiles used in medical, sports, and hygiene applications are highly susceptible to microbial contamination due to frequent exposure to moisture, bodily fluids and environmental microorganisms, resulting in odor formation, staining, compromised hygiene and fiber degradation [1]. For example, sweat-soaked sportswear provides an ideal environment for bacterial proliferation, causing odor and skin irritation. Likewise, uncontrolled microbial growth in everyday hygiene products, such as towels or bedding, can result in malodor and material deterioration, thereby requiring more frequent laundering and replacement. These issues underscore the critical need for effective antibacterial treatments on textile surfaces to preserve cleanliness, prevent malodor, and extend service life.

The consequences of microbial contamination are more severe in healthcare settings, where textiles, including bed linens, patient gowns, uniforms, and wound dressings, can be vectors for pathogenic bacteria if not properly sanitized [2], thereby contributing to hospital-acquired infections, threatening patient safety, and increasing healthcare costs [3]. The use of antimicrobial-finished textiles in hospitals, clinics, and

* Corresponding authors.
E-mail addresses: valentina.trovato@unibg.it (V. Trovato), giulia.rando@cnr.it (G. Rando), mariarosaria.plutino@cnr.it (M.R. Plutino).
[1] These authors contributed equally to this work.
[2] These authors jointly supervised this work.

https://doi.org/10.1016/j.surfin.2026.110232
Received 22 December 2025; Received in revised form 13 July 2026; Accepted 27 July 2026
Available online 28 July 2026

care facilities can help mitigate the spread of infectious agents, including drug-resistant bacteria, by continuously inhibiting microbial growth on frequently touched surfaces, thereby protecting both patients and healthcare workers [4]. Similarly, in everyday settings, antibacterial athletic apparel, hygienic wipes, and diapers can reduce local bacterial growth and improve protection against rashes and infections. Thus, preventing microbial proliferation on textile products is crucial for curbing infection and maintaining hygiene [5].

Various antibacterial finishing methods have been developed for textiles using chemical, biological, and nanotechnological approaches. Traditional approaches rely on the application of chemical antimicrobials, including quaternary ammonium salts, polyhexamethylene biguanide, triclosan, and N-halamine compounds, as coatings or binders on textile fibers, conferring biocidal properties [6]. These agents offer broad-spectrum microbicidal or microbiostatic activity by disrupting cell membranes or metabolic processes. For instance, triclosan and polyhexamethylene biguanide have long been used to treat textiles for medical applications, and chitosan (a natural biopolymer) has been employed as a bio-based antimicrobial finish [7]. Physical finishing techniques have also been explored, such as plasma treatment or ultraviolet (UV) irradiation, to graft antimicrobial polymers onto fabrics or deposit metallic films through processes such as magnetron sputtering [8], without significantly altering the underlying material properties.

In recent years, nanotechnology-based approaches have emerged as advanced solutions for antimicrobial textiles. Embedding nanomaterials, particularly metallic and metal-oxide nanoparticles, into cotton and other textiles provides durable and effective antibacterial properties due to the high surface area and unique reactivity of these nanoparticles [9]. Silver nanoparticles (AgNPs) are the most widely used because of their strong, broad-spectrum antibacterial and antifungal efficacy. Techniques for incorporating AgNPs into cotton have been refined over the past two decades, including in situ synthesis on the fiber and nanoparticle coating [10]. Other nanoscale additives, such as titanium dioxide (TiO_2) and zinc oxide (ZnO), provide dual functionality, namely UV protection and antibacterial action [10–12]. However, as photocatalytic agents, they typically require UV activation, thereby limiting their usefulness in medical textiles that are predominantly used indoors.

Although these antibacterial agents are generally effective, they have important drawbacks. The primary concern is bacterial adaptation. For example, widespread use of AgNPs has been associated with the development of Ag-tolerant bacterial strains [13]. It has been demonstrated that chronic, low-level exposure can stimulate bacterial stress responses, which in turn leads to the secretion of extracellular polymeric substances and other biofilm components, thereby reducing the effectiveness of AgNPs [14]. Similarly, the extensive use of chemical biocides, including triclosan and quaternary ammonium compounds (QACs), in consumer products and textiles is believed to accelerate the development of more resistant microbial populations [15].

Toxicological and environmental impacts further complicate the ongoing use of these agents. Persistent synthetic antimicrobials, such as triclosan, have been shown to bioaccumulate, thereby threatening aquatic ecosystems and causing a range of health concerns, including skin irritation and endocrine disruption [15]. It is important to note that heavy-metal-based systems present similar hazards: AgNP-treated fabrics release silver ions and particles during routine laundering, contaminating wastewater streams and ultimately affecting the wider environment [16,17]. Considering the ecological and safety concerns associated with these substances, several authorities now recommend restricting silver-based antimicrobials to essential medical uses, such as wound dressings, while efforts to identify safer alternatives are being intensified [18].

Recently, the United States Environmental Protection Agency (EPA) has officially recognized copper as the first, and so far, the only, metallic surface approved for antimicrobial activity, demonstrating at least a 99.9% reduction of most pathogens within two hours of contact. This effectiveness rivals that of much more expensive bactericidal metals, including silver and gold [19].

In this regard, copper nanoparticles (CuNPs) have garnered considerable interest across various scientific disciplines due to their unique physicochemical and electronic properties, as well as their broad applicability, which distinguishes them from bulk copper [20]. Notably, CuNPs have a high surface area-to-volume ratio, which enhances their reactivity and interactions with other substances. Furthermore, their high thermal and electrical conductivity makes them valuable in nanoelectronics, catalysis, sensors, and biomedicine [20]. Because copper plays essential biological roles, a daily intake of approximately 900 μg of copper is recommended for healthy adults. However, although copper is essential for many physiological processes, excessive exposure can cause toxic effects. Notably, its strong antimicrobial efficiency and cost-effectiveness, often comparing favorably with other metal-based agents such as silver, have led to its extensive use in biomedical and industrial fields [21]. The bactericidal action of copper compounds is thought to mimic the catalytic mechanisms of natural enzymes in the human body, thereby enhancing their appeal for use in nanozyme-based antibacterial platforms [22]. In textile applications, nanoscale copper particles exhibit potent antibacterial action through multiple mechanisms, making it difficult for bacteria to develop resistance [23,24]. Numerous methods have been developed for the efficient synthesis of CuNPs while maintaining precise control over size, shape, and surface properties [20–25], including thermal decomposition [26], solution reduction with mild reductants [27], or electrochemical methods such as liquid-phase plasma reduction [28]. Additional reported routes include photoreduction [29], microemulsion techniques [30], microwave-assisted synthesis [31], and laser ablation [32]. Among copper-based compounds, copper(I) species have been reported to exhibit greater antibacterial activity than metallic copper and copper(II) compounds [19].

Copper-based antibacterial finishing of cotton fabrics has been widely investigated, but the reported systems differ markedly in terms of copper phase, deposition route, and durability strategy. Earlier work by Perelshtein et al. described CuO–cotton nanocomposites prepared by ultrasound-assisted deposition, demonstrating that copper oxide can be effectively immobilized on cotton and impart antibacterial activity [33]. Rezaie et al. later reported an environmentally friendly route for the functionalization of cotton with CuO, achieving excellent antibacterial performance and additional photocatalytic functionality [34].

In a durability-oriented approach, Agrawal et al. used silane coupling agents to anchor CuO nanoparticles onto cotton, achieving antibacterial efficacy of up to 99% and good resistance to washing and abrasion [9]. More recently, Zhu et al. prepared broad-spectrum antibacterial cotton by in situ synthesis of Cu_2O particles in a PDMS-based medium [35].

Among copper-based materials, cuprous iodide (CuI) offers distinct advantages for coating applications, including its colorless appearance, skin compatibility, environmental stability in air and aqueous conditions, and rapid germicidal action [36,37]. In particular, copper(I) iodide (CuI) is especially effective for biomedical applications, including wound dressings, because of its greater antimicrobial performance than that of its copper(II) counterparts [21]. Recent studies have demonstrated that CuI nanoparticles exhibit both broad-spectrum antimicrobial and antiviral activity [19]. Moreover, it has been reported that CuI-based particles may promote reactive oxygen species (ROS) generation in Gram-negative and Gram-positive bacterial cells, contributing to DNA damage and suppression of gene transcription [38]. The same ROS also compromise viral integrity by disrupting capsid proteins and degrading the viral genome, ultimately abolishing infectivity. Beyond these bioactive properties, CuI is an inorganic p-type semiconductor with versatile coordination chemistry, which permits facile association with a wide range of organic ligands, thereby enabling the construction of hybrid organic–inorganic materials. Improving the structural and chemical quality of these CuI-based hybrids is expected to expand their use in optoelectronic and photonic devices. Consequently, significant

effort has been directed toward growing high-purity CuI single crystals, including chemical precipitation, sonication, coprecipitation, and microwave-assisted hydrothermal methods [39–43]. Despite their effectiveness, these approaches often involve hazardous precursors, multi-step procedures, and elevated temperatures, thereby increasing production costs and limiting environmental and biological safety [44]. As more sustainable and environmentally friendly alternatives, green synthesis methods have gained significant attention because they minimize the use of toxic reagents, lower energy requirements, and employ benign solvents such as water, ethanol, or ethyl acetate [44], or plant extracts instead of harsh chemicals [45,46]. Nonetheless, the low solubility of CuNPs in aqueous solutions and their strong van der Waals forces lead to inhomogeneous structures, posing significant challenges in preventing nanoparticle agglomeration in aqueous solutions used for textile finishing. To stabilize CuNPs and enhance their compatibility with aqueous systems, polymeric matrices are often employed. Several polymeric matrices are favored in this context owing to their ready availability, the straightforward routes by which they can be assembled from low-molecular-weight precursors, their intrinsic water solubility, and their compatibility with physiological environments [47]. Polyvinyl alcohol (PVA; $-[CH_2–CHOH]_n-$) is a notable example, as an environmentally benign, water-soluble vinyl polymer [48]. Numerous studies have described the formation of binary coordination complexes between PVA and divalent metal ions, such as Cu(II), Co(II), Ni(II), and Zn(II) [49,50]. Unlike other self-templating organic matrices, PVA chelates metal cations through its pendant hydroxyl groups, leading to their physical and/or chemical entrapment within the polymer network, thus acting as a nanoparticle stabilizer. These approaches give copper-containing finishes a more sustainable profile, aligning with the growing demand for sustainable textile processing.

In recent years, the sol–gel technique has been extensively studied for textile finishing due to its tunable properties and lower health risks than many conventional systems [51,52]. Typically, metal–organic compounds or inorganic metal salts serve as precursor materials, enabling the transition from a liquid (predominantly colloidal) “sol” phase to a solid “gel” phase [53]. This technique has been explored for innovative textile applications, enabling multifunctional coatings with properties such as electrical conductivity [54], self-cleaning [55,56], flame retardancy [57,58], water repellency [56,59,60], hydrogen production via water photo-splitting [61], and stimuli-responsive behavior [62,63].

In this study, to develop a scalable, cost-effective, and straightforward antibacterial finish for cotton fabrics, CuI–PVA particles were prepared and dispersed into a GPTMS/TEOS-derived hybrid sol–gel formulation that could be applied by a conventional pad–dry–cure process, with the aim of combining antibacterial effectiveness with coating cohesion under the investigated laundering conditions. To the best of our knowledge, no studies have reported treating textile materials with CuI–PVA using conventional finishing methods. The precision and continuity of this method make it particularly suitable for industrial scale-up, effectively overcoming the limitations of other techniques, especially when inorganic compounds with low solubility and dispersibility in water are used in textile finishing [64–66].

The CuI–PVA suspension and its mixture in a sol–gel silica–mediated coating on cotton were characterized using ATR-FTIR and SEM-EDS to assess the chemical structure and surface features. The treated textiles were evaluated against representative Gram-positive (*S. aureus*) and Gram-negative (*E. coli*) microorganisms to assess their potential for infection control. Considering the well-documented broad-spectrum antimicrobial properties of copper iodide [19,21,36,37,67], this approach offers a promising proof-of-concept strategy to demonstrate its antimicrobial efficacy, with potential applications in cellulose-based garments, such as sportswear and medical textiles for hospitals and patients, particularly in response to emerging infectious disease threats.

2. Experimental section

2.1. Materials

ISO 105-F02 cotton fabric (hereafter, CO) was obtained from Testfabrics (West Pittston, PA, USA). Electrolytic-grade copper plates (purity 99.999%) were employed in the synthesis. All experimental procedures were conducted under ambient atmospheric conditions. Prior to use, copper substrates were thoroughly cleaned and then rinsed with triple-distilled water before immersion in the chemical bath. Tetraethyl orthosilicate (TEOS, Acros Organics, 98% purity) and (3-Glycidyloxypropyl)trimethoxysilane (GPTMS, VWR Chemicals, 98% purity) were used as sol–gel precursors. Polyvinyl alcohol (PVA, Mw: 13,000–23,000, partially hydrolyzed), iodine, ethyl alcohol, glacial acetic acid, and hydrochloric acid (all reagent grades) were purchased from Merck (Milan, Italy) and used as received without further purification.

The antibacterial tests were performed using bacteria obtained from the American Type Culture Collection (ATCC): Gram-positive bacteria, *S. aureus* ATCC 6538 and Gram-negative bacteria, *E. coli* ATCC 11229 (supplied by Biogenetics Diagnostics Srl, Italy).

2.2. Synthesis of CuI–PVA particles

Copper(I) iodide (CuI) particles were synthesized using a sonochemical method as a simple, environmentally benign, and efficient route under mild conditions. Stoichiometric amounts of metallic copper powder (Cu, ≥99% purity; 72.4 mmol) and molecular iodine (I_2, ≥99% purity; 26.8 mmol) were added to absolute ethanol (EtOH, 100 mL) in a glass beaker. The resulting suspension was subjected to continuous ultrasonic irradiation in a sonicator bath (40 kHz, 100 W) for approximately 15h at room temperature (25°C). During sonication, a progressive decolorization of the solution was observed, consistent with iodine consumption and indicating reaction progress, as described in Eq. (1):

$$2Cu + I_2 \rightarrow CuI \quad (1)$$

Upon completion of the reaction, the unreacted bulk copper was readily removed by carefully decanting the liquid phase. The resulting suspension was subsequently centrifuged at 6000 × g for 10 min to isolate the solid from the supernatant. The collected CuI particles were washed three times with absolute ethanol; after each washing step, the suspension was allowed to settle and the supernatant was decanted until it became colorless, thereby promoting the removal of residual iodine-containing species. For colloidal stabilization, the purified CuI particles were dispersed in a 2% (w/v) aqueous poly(vinyl alcohol) (PVA) solution, adjusted to pH ≈ 9 with a phosphate buffer. The mixture was stirred until a homogeneous colloidal dispersion was obtained.

2.3. Synthesis of GPTMS–TEOS sol

TEOS (10.1 mmol) was added to a minimal volume of deionized water under continuous magnetic stirring at room temperature. Subsequently, an appropriate amount of glacial acetic acid, equivalent to 277.3 mmol, was added dropwise to the TEOS solution to ensure complete hydrolysis and acid-catalyzed condensation of the alkoxysilane at a pH of around 2.5. Upon obtaining a clear, homogeneous acidic TEOS solution, GPTMS (15.2 mmol) was introduced gradually while stirring, maintaining a TEOS:GPTMS molar ratio of 2:3. The resulting solution was stirred for an additional 30 min to ensure homogeneity, followed by the addition of the final required amount of deionized water. After 4 h of stirring at room temperature, a clear sol–gel solution with a final concentration of 0.05 M (GPTMS–TEOS or GT) was obtained.

In this binary silane system, the two precursors were selected because they perform complementary functions. TEOS primarily acts as the inorganic network former and, upon hydrolysis and condensation, generates the main Si–O–Si siloxane backbone responsible for the

cohesion and structural stability of the coating. GPTMS, in contrast, acts as an organofunctional coupling precursor: while its trimethoxysilane groups participate in the same sol–gel condensation reactions, its glycidoxypropyl moiety increases the organic character of the network and improves interfacial compatibility with both the hydroxyl-rich cotton surface and the PVA-stabilized CuI phase. The combined use of TEOS and GPTMS was therefore intended to obtain a hybrid coating in which rigidity and film-forming ability are balanced with adhesion and interfacial integration.

2.4. Preparation of hybrid sol–gel CuI–PVA

Two formulations, hereafter coded as GT CuI–PVA 2% and GT CuI–PVA 4%, were prepared by dispersing different amounts of CuI–PVA in the 0.05 M GPTMS–TEOS sol. The CuI–PVA content was calculated as a weight percentage relative to the total mass of the finishing dispersion, according to the following expression:

$$CuI-PVA\ (wt\%) = \frac{m(\mathrm{CuI-PVA})}{m(\mathrm{CuI-PVA}) + m(\mathrm{sol-gel})} \times 100 \quad (2)$$

where m(CuI–PVA) is the mass of the CuI–PVA phase added to the formulation and m(sol–gel) is the mass of the GPTMS–TEOS sol. On this basis, the two final dispersions contained 2.04 wt% and 4.08 wt% CuI–PVA, respectively. For simplicity, they were labeled as 2% and 4% throughout the manuscript. It should be noted that these values refer to the composition of the application bath, whereas the add-on values on the treated fabrics were determined separately after the pad–dry–cure process and are reported in the Supplementary Material.

The finish is classified as a hybrid material because it combines organic and inorganic components in a single coating architecture. Although hydrolysis and condensation generate an inorganic Si–O–Si siloxane framework, the use of GPTMS also introduces a non-hydrolyzable glycidoxypropyl organic moiety into the network. As a result, the matrix is more appropriately described as an organosiloxane hybrid phase. Moreover, this matrix incorporates the CuI–PVA particulate phase, in which CuI is the inorganic antibacterial component and PVA is the organic stabilizing component. Therefore, the deposited finish is hybrid in both its matrix chemistry and its overall multicomponent architecture. This usage is consistent with the sol–gel literature on organic–inorganic hybrid materials and GPTMS/TEOS-derived hybrid coatings [68–70].

2.5. Coating procedure and washing tests

Both dispersions were applied separately to cotton fabrics using a two-roll laboratory padder (Werner Mathis, Zurich, Switzerland) operating at a nip pressure of 2 bar. The wet pick-up (%) was calculated according to Eq. (3),

$$Wet\ pick-up(\%) = \frac{(W_w - W_i)}{W_i} \times 100 \quad (3)$$

where (W_i) and (W_w) represent the dry mass of the specimen before finishing and the wet mass of the specimen after application, respectively. Five replicate measurements were performed, and the results are reported as mean ± standard deviation (SD) in the corresponding tables and figures.

The treated fabrics were dried at 80°C for 5 min and then cured at 160°C for 2 min in a laboratory oven. As a control, cotton fabrics were also treated with the GPTMS–TEOS sol–gel solution alone, without CuI–PVA, and processed identically.

Before all experiments, the samples were conditioned under a standard atmosphere of 65 ± 4% relative humidity and 20 ± 2°C for at least 24 h. The add-on values for the coated samples were determined as reported in Eq. (4),

$$A\ (\%) = \frac{(W_f - W_i)}{W_i} \times 100 \quad (4)$$

where (W_i) and (W_f) represent the dry mass of the specimen before and after finishing, curing, and conditioning, respectively. For each sample, five replicates were taken, and the mean value was calculated.

To assess durability, the coated fabric samples underwent one and three washing cycles in accordance with the ISO 105-C10:2006 method. The samples were immersed in a 2 g·L^{-1} soap solution, preheated to 40 °C, and maintained at a liquor ratio of 30:1 for 30 min in a Mathis Labomat (Werner Mathis Zurich, Switzerland). Following each wash cycle, the samples were dried in a forced-air oven at 105 ± 3 °C until a stable mass was achieved (defined as a change of ≤0.1 mg between two consecutive weighings, which, for the fabric used, typically took 90 min), then cooled to room temperature in a desiccator over fresh silica gel and weighed to the nearest 0.1 mg. The percentage weight loss of washed fabrics (WLW, wt%) with respect to the unwashed samples was calculated according to Eq. (5):

$$WLW\ (\%) = \frac{(W_{TW} - W_T)}{W_T} \times 100 \quad (5)$$

where (W_T) and (W_{TW}) denote the dry mass of the treated fabrics before and after multiple ISO 105-C10 washing cycles, respectively. For each property, five replicates were taken, and the results are reported as mean ± SD.

2.6. Characterization techniques

The hydrodynamic diameter and size distribution of particles in the colloidal solutions, expressed through the polydispersity index (PDI), were measured using a DLS instrument (Zetasizer Pro, Malvern Instruments, Worcestershire, UK) at 25°C, using a scattering angle of 173° and a laser wavelength of 633 nm (He-Ne) with a power of 4 mW. The refractive indices were 1.33 and 2.35 for the medium and the CuI particles, respectively. Additionally, zeta potential measurements were carried out on both GT CuI–PVA 2% and 4% using the same equipment. Before DLS and zeta potential analysis, suspensions were sonicated for 30 min using an ultrasonic bath. Subsequently, 100 µL of each suspension was diluted with 1 mL of Milli-Q water.

Fourier transform infrared (FTIR) spectroscopy was performed using the attenuated total reflection (ATR) technique with a Thermo Avatar 370 spectrophotometer (Thermo Nicolet, Madison, WI, USA) equipped with a diamond crystal. Spectral measurements were recorded over the range of 4000–600 cm^{-1} with a spectral resolution of 4 cm^{-1} and 64 scans per sample. Data acquisition and analysis were conducted using Omnic v7.3 software and processed with Origin v7.0. The spectra of sol–gel-based CuI–PVA dispersion, acquired on dried xerogel, were reported in Transmittance. The spectra of the untreated and treated fabrics were normalized to the absorption band at 1315 cm^{-1}, associated with the C–H bending mode of cellulose.

Raman spectroscopy was performed in the spectral range of 0–3900 cm^{-1} using an XploRA Plus Raman spectrometer (HORIBA, Kyoto, Japan) equipped with a 600 groove/mm diffraction grating. A Cobolt 532 nm laser served as the excitation source, focusing through a 100 × objective (NA 0.9) and delivering approximately 100 mW at the specimen surface. For each spectrum, an acquisition time of 10 s was employed with two accumulations. The most representative spectra were selected for analysis and presentation, and each sample was measured in triplicate to ensure reproducibility. Before comparative analysis, all Raman spectra underwent baseline correction, while for cotton samples a further min–max normalization was achieved.

The surface morphology of CuI–PVA, untreated and treated textiles was observed using a scanning electron microscope (SEM, Phenom ProX G6 Desktop SEM, Thermo Fisher Scientific, Waltham, MA, USA) equipped with energy-dispersive X-ray spectroscopy (EDS) under high

vacuum at an accelerating voltage of 10 kV. The samples were affixed to aluminum sample holders using a graphite adhesive.

Thermogravimetric analysis (TGA) of the samples was performed using Discovery TGA 550 (TA Instruments, New Castle, DE, USA). The temperature ramp was set from 25 to 750°C at a heating rate of 10°C/min, with a flow rate of 90 mL/min and a balance flow of 10 mL/min, respectively. The analyses were conducted under an air atmosphere. The experimental error was ±0.5% for weight and ±1°C for temperature.

The color assessment of treated samples was conducted using a spectrophotometer (Spectro 700; Datacolor, Giussano, Italy) following ISO 105-J02:1997 [71] and ISO 105-J03:2009 [72] based on the CIE L*a*b* coordinate system, where L*, a*, and b* represent lightness–darkness, red–green, and yellow–blue values, respectively. Similarly, ΔL*, Δa*, and Δb* denote the differences in each parameter relative to a reference standard fabric. The overall color difference (ΔE^*) was calculated using Eq. (6):

$$\Delta E^* = \sqrt{(\Delta L^*)^2 + (\Delta a^*)^2 + (\Delta b^*)^2} \quad (6)$$

Spectral reflectance measurements were recorded across the visible spectrum, using a SAV 9 mm aperture, ranging from 400 to 700 nm, and subsequently converted into CIE L*a*b* color coordinates based on a D65 illuminant and a viewing angle of 10°, using Datacolor TOOLS v1.1 software. Furthermore, according to the Color Measurement Committee system, a ΔE^* value < 1 is the threshold below which samples are considered to have the same color as the reference.

Calibration was conducted with specular inclusion, a small-area view, and the UV filter set to OFF.

The whiteness index (W_{CIE}) was calculated using Eq. (7):

$$W_{CIE} = Y + 800 \times \left(x_n - \frac{X}{X+Y+Z}\right) + 1700 \times \left(y_n - \frac{Y}{X+Y+Z}\right) \quad (7)$$

where X (related to red/green sensitivity), Y (the luminance), and Z (the blue sensitivity) are the tristimulus values, and x_n and y_n are the chromaticity coordinates for the diffuser under D65.

2.7. Assessment of antibacterial properties

The antibacterial activity of both blank (unloaded) and CuI–doped siloxane-based materials was assessed against *S. aureus* ATCC 6538 (Gram-positive) and *E. coli* ATCC 11229 (Gram-negative) strains. Testing was conducted both before and after the materials were applied to the cotton fabric.

Antibacterial performance was evaluated according to the ASTM E2149-25 procedure "Standard test method for determining the antimicrobial activity of immobilized antimicrobial agents under dynamic contact conditions" [73]. A bacterial culture was incubated for 24 h in a nutrient broth (buffered peptone water for microbiology, VWR Chemicals, Milan, Italy) (bacterial inoculum) with a buffer at pH 7.0, achieving a working concentration of 1.5–3.0 × 10^5 colony-forming units (CFU)/mL, as determined using spectrophotometric analysis.

The bacterial inoculum was then exposed to the antibacterial materials under shaking at 190 rpm at room temperature for 1 h, maintaining an antibacterial material-to-inoculum ratio of 1:50 (w/v). Following incubation, 1 mL of the inoculum was diluted 1000-fold with buffer to achieve a final concentration of 1.5–3.0 · 10^2 CFU · mL^{-1} and subsequently plated in 15 mL of Yeast Extract Agar (Sigma Aldrich). The inoculated plates were incubated at 37°C for 24 h, after which the surviving bacterial colonies were quantified using the plate count method.

Antibacterial activity was expressed as a percentage reduction in bacterial colonies after contact with the test specimen relative to the initial bacterial load in the control plate, as described by Eq. (8):

$$\%\, bacterial\, reduction = \frac{B - A}{B} \times 100 \quad (8)$$

where A represents the CFU · mL^{-1} after exposure to the test specimen, and B denotes the CFU · mL^{-1} at the initial contact time (inoculum control). The tests were conducted in triplicate, using independent microbial cultures for each antimicrobial assay. Data are presented as mean values ± standard deviation (SD). The two-way ANOVA test, with the Sidak correction, was used to perform significance analysis. p-values lower than 0.05 were considered statistically significant. Data were analyzed with "GraphPad Prism" software, version 8.0.2 (GraphPad, Inc., San Diego, CA, USA).

2.8. Assessment of textile properties

The stiffness of the coated cotton fabrics was investigated as a representative parameter of their textile properties, since variations in stiffness provide useful information on changes in fabric softness. This mechanical property is mainly affected by fabric-related factors, including yarn count, weave structure, and areal density. Textile stiffness was determined by measuring the bending length (LB) according to DIN 53362 [74]. In this procedure, a fabric strip with dimensions of 10.0 cm × 2.5 cm was moved, together with a measuring bar, over the edge of a fixed horizontal support. When the fabric bent under its own weight beyond an angle of 41.5°, the corresponding overhang length was recorded. The bending stiffness (B), expressed in $cN{\cdot}cm^2$, was then calculated according to Eq. (9):

$$B = 0.00981 \times m \times L^3 \quad (9)$$

where m is the fabric mass per unit area, expressed in $g{\cdot}cm^{-2}$, and L is the measured overhang length, expressed in cm. For each sample, measurements were carried out in two directions, and the mean values were calculated from five replicates.

3. Results and discussion

3.1. CuI–PVA particles: synthesis and incorporation into a hybrid sol–gel matrix

In this work, CuI particles were synthesized through a simple, environmentally friendly, one-step sonochemical process conducted at room temperature (Fig. 1). The sonochemical method uses high-frequency ultrasonic waves to generate acoustic cavitation within the liquid reaction medium. This process involves the formation, growth, and violent collapse of microbubbles, creating localized transient hot spots characterized by extreme temperatures and pressures. These conditions significantly enhance the kinetic energy of reactants, promoting rapid nucleation as well as inducing morphological and compositional transformations in the forming nanoparticles through intense interparticle collisions.

For stabilization and subsequent application, the purified CuI particles were redispersed in an aqueous polyvinyl alcohol (PVA) solution (2% w/v), with the pH adjusted to 9 by phosphate buffer. PVA, a water-soluble polymer with a hydrophobic carbon backbone and hydrophilic pendant hydroxyl groups, plays a critical role in stabilizing the CuI particulate phase. In aqueous solutions, the polymer adopts conformations where the hydroxyl groups remain highly solvated and available for interactions. Under mildly alkaline conditions, partial deprotonation of these groups generates nucleophilic PVA–O^- sites capable of coordinating copper ions. These donor–acceptor interactions promote the in-situ formation and stabilization of Cu(I) iodide, resulting in the formation of cationic PVA–CuI complexes (formally PVA–Cu(I)). The resulting dispersions showed good colloidal stability, with no observable precipitation or particle aggregation during storage or processing.

To further enhance their functional properties, two formulations (GT CuI–PVA 2% and GT CuI–PVA 4%) were prepared by dispersing CuI–PVA particles within a sol–gel matrix derived from GPTMS ((3-glycidyloxypropyl)trimethoxysilane) and TEOS (tetraethyl

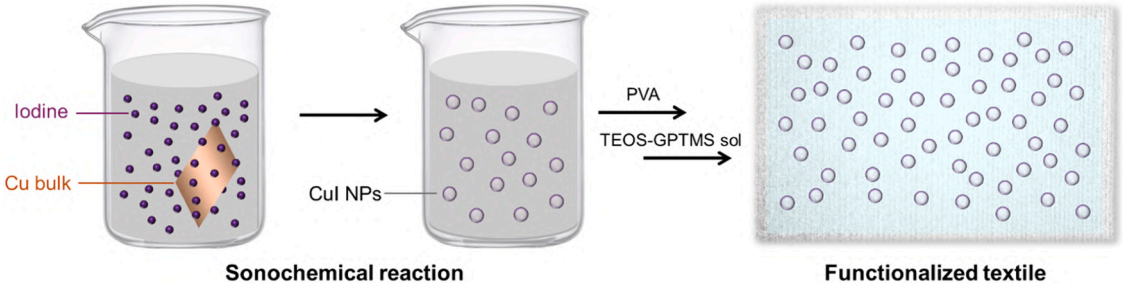

Fig. 1. Formation of CuI–PVA particles by sonochemical reaction and their incorporation into a hybrid CuI–PVA/siloxane sol–gel finishing for cotton fabrics.

orthosilicate). The use of these two silicon precursors was deliberate, as they fulfill distinct but complementary roles in the hybrid coating. TEOS mainly contributes to the formation of the inorganic siloxane network, providing the coating with structural continuity and cohesion. GPTMS, in addition to participating in the condensation process through its alkoxysilane groups, introduces an organofunctional glycidylpropyl segment that improves compatibility with the organic components of the system, namely cotton cellulose and the PVA shell surrounding the CuI particles. In this way, the GPTMS/TEOS combination promotes the formation of a hybrid matrix that uniformly disperses the CuI–PVA phase and facilitates its anchoring onto the textile substrate. The inherent colloidal stability of CuI–PVA further supported its homogeneous incorporation into the sol–gel system, resulting in a functional coating suitable for cotton finishing.

The colloidal stability of the CuI–PVA particles favored their uniform dispersion within the sol–gel matrix, producing a hybrid functional Cu-based sol–gel finishing (Fig. 1). This composite material was therefore considered suitable for deposition onto cotton fiber substrates and for subsequent evaluation as a proof-of-concept antibacterial textile finish.

3.2. Characterization of CuI–PVA structures

3.2.1. SEM-EDS of CuI–PVA particles

Scanning electron microscopy (SEM) shows that the CuI–PVA phase consists of compact aggregates that are predominantly submicrometric, with typical projected dimensions of a few hundred nanometers to approximately 1 μm, and with some coalesced aggregates extending into the low-micrometer range (Fig. 2a and 2b). Owing to the partial overlap and close packing of adjacent particles, the SEM analysis should be regarded as semi-quantitative, yet it clearly indicates that the CuI–PVA phase is not present as a continuous bulk deposit, but rather as a particulate system made of compact aggregates. This morphology is favorable for textile finishing because it can promote relatively uniform surface coverage and efficient incorporation within the sol–gel-derived matrix. In addition, the EDS elemental analysis (Fig. 2c) confirmed the presence of Cu and I as the main inorganic components, with minor C and O contributions attributable to the PVA stabilizer and no significant elemental impurities.

While EDS confirms the elemental composition of the inorganic phase, it does not provide crystallographic information on its own. Therefore, definitive phase identification requires a complementary diffraction technique such as XRD.

3.2.2. Chemical structure analysis of sol–gel dispersed CuI–PVA particles

Fig. 3 compares the FTIR spectra of the pristine GT, the CuI–PVA powder, and the hybrid xerogels loaded with 2.04 and 4.08 wt% CuI–PVA, indicating the successful formation of the siloxane network and the effective incorporation of CuI–PVA particles. The GT spectrum is dominated by the Si–O–Si asymmetric stretching band at 1021 cm^{-1} [66], accompanied by the characteristic Si–OH deformation at 918 cm^{-1} and the Si–O–Si symmetric stretching and rocking modes at 779 and 676 cm^{-1}, respectively, confirming extensive condensation of the silanes into a three-dimensional network [67,75]. The broad band centered at 3324 cm^{-1} corresponds to ν(OH) from residual silanols and adsorbed water, whereas the bands at 2936 and 2873 cm^{-1} originate from the $–CH_2–$ groups of the GPTMS propyl spacer. No signals attributable to unreacted epoxy rings at 3057 cm^{-1} (asymmetric C–H stretch), 2999 cm^{-1} (symmetric C–H stretch), 1255 cm^{-1} (ring breathing), 907 cm^{-1} and 840 cm^{-1} (asymmetric and symmetric ring deformation) are present in the FTIR spectra of cross-linked films, confirming that the epoxide rings have reacted and the organo-silica precursors have undergone cross-linking within the hybrid network [76].

For CuI–PVA powder, besides the expected ν(OH) and ν(CH) bands of PVA [77], the spectrum exhibits three discrete absorptions absent in the pristine xerogel: a broad band between 2600 and 2400 cm^{-1}, assigned to CO_2 vibronic modes and two sharp bands at 2035 and 1978 cm^{-1} (highlighted by dotted rectangles) attributed to higher-order Cu-I lattice vibrations, thus confirming the presence of the CuI particles [78]. The spectroscopic features indicate an electron-rich, heterogeneous surface that supports pronounced metal→CO π-back-donation [79], thereby providing evidence for the successful formation of the PVA-stabilized CuI particles.

In the hybrid xerogels, arising from the integration of inorganic siloxane domains, GPTMS–derived organic moieties, and the organic/inorganic CuI–PVA particulate phase, the Si–O–Si stretching region (1200–1000 cm^{-1}) retains its overall profile and intensity, indicating

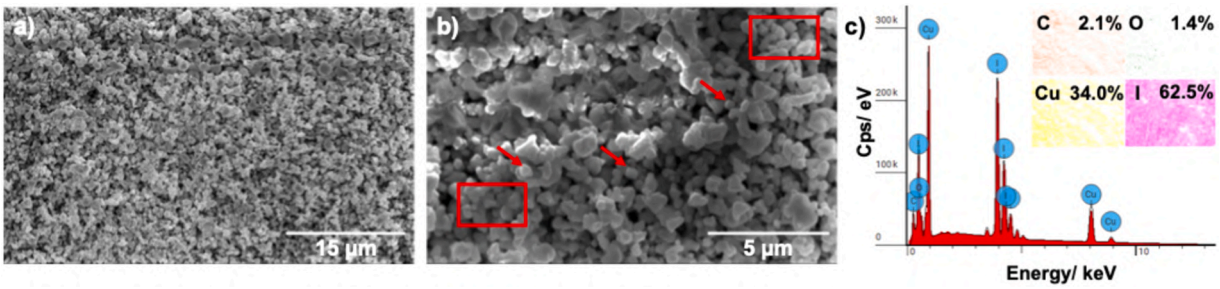

Fig. 2. (a) Low-magnification SEM image of CuI–PVA particles showing their overall distribution; (b) higher-magnification SEM image highlighting the rounded morphology (red arrows) and aggregation state (red rectangles); (c) EDS-based elemental analysis and elemental mapping of CuI–PVA.

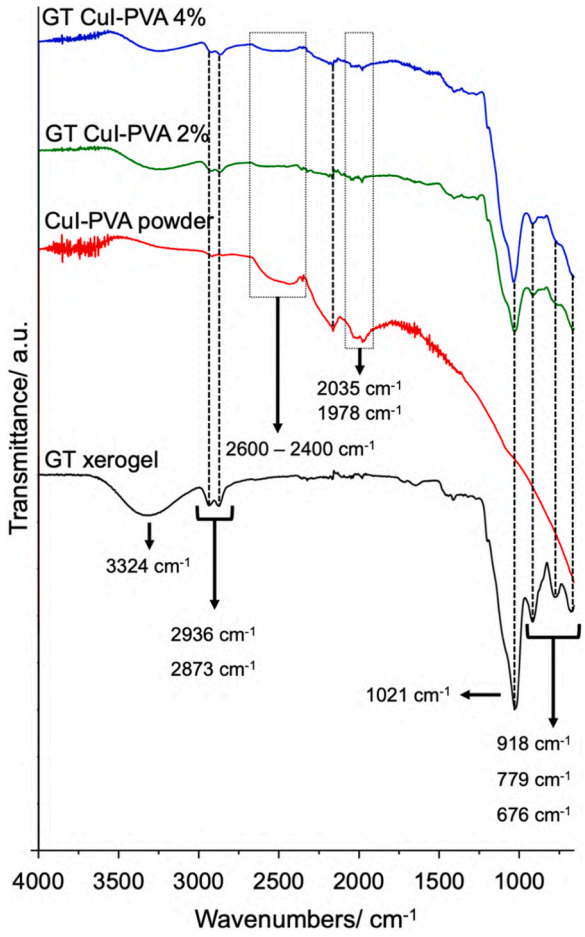

Fig. 3. FTIR spectra of GPTMS–TEOS xerogel (black curve), CuI–PVA powder (red curve), and GPTMS–TEOS xerogel embedding CuI–PVA particles at 2.04 wt % and 4.08 wt% (green and blue curves, respectively).

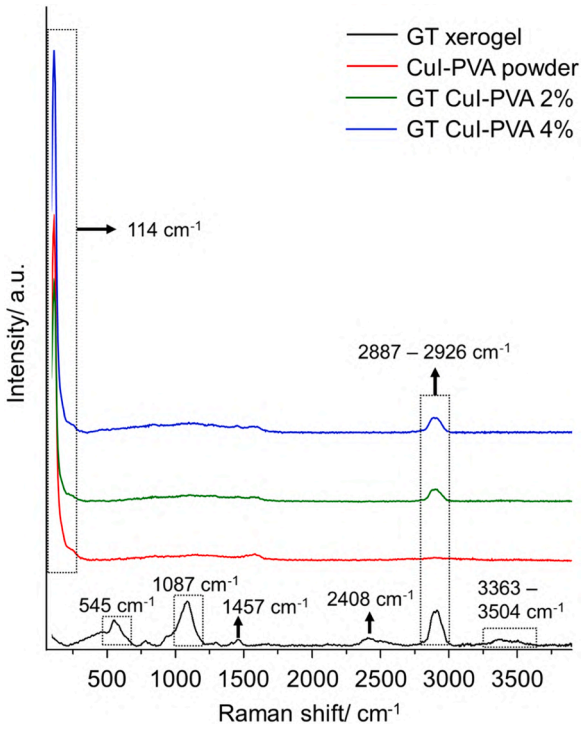

Fig. 4. Raman spectra of GPTMS–TEOS xerogel (black curve), CuI–PVA (red curve), and GPTMS–TEOS xerogel embedding CuI–PVA particles at 2.04 wt% and 4.08 wt% (green and blue curves, respectively).

that the inorganic siloxane framework is not substantially altered by the CuI–PVA addition.

Concomitantly, the ν(CH) bands at 2936–2873 cm^{-1} increase in intensity in proportion to the CuI–PVA loading, reflecting the higher aliphatic content supplied by PVA. The CuI particle signatures at 2035 and 1978 cm^{-1} remain detectable in both composites, albeit attenuated relative to the powder, confirming that the particles survive the sol–gel process. Notably, the ν(OH) band of the hybrid xerogels becomes broader and shifts slightly to lower wavenumbers with respect to the pristine matrix, suggesting additional hydrogen-bonding interactions between residual silanols and the hydroxyl groups of PVA, which may favor the physical integration of the CuI–PVA phase within the hybrid xerogel. The FTIR data collectively support (i) the preservation of the inorganic siloxane backbone, (ii) the retention of the CuI–PVA spectroscopic signature after dispersion in the sol–gel matrix, and (iii) the occurrence of hydrogen-bonding interactions within the hybrid xerogel. These findings provide a chemical framework for the coating system subsequently evaluated on cotton fabrics.

Fig. 4 illustrates the Raman spectra of the pristine GPTMS–TEOS xerogel (GT, black line), the CuI–PVA powder (red), and the hybrid xerogels containing 2.04 wt% and 4.08 wt% CuI–PVA (green and blue, respectively).

The GT xerogel displays the characteristic siloxane network, exhibiting an intense ν_{as}(Si–O–Si) band at 1087 cm^{-1}, which signifies a densely cross-linked siloxane backbone [80]. The δ(Si–O–Si) ring vibration at 545 cm^{-1} signals the presence of small three-membered siloxane rings [81,82], while the presence of organic integrity is indicated by the CH_2 scissoring at 1457 cm^{-1} [83] and the ν(CH_2) envelope at 2887-2926 cm^{-1} [84]. A weak overtone at 2408 cm^{-1} further supports extended Si–O–Si coupling [81]. Finally, the broad 3363–3504 cm^{-1} ν(OH) band is indicative of residual silanols [85].

The CuI–PVA powder, by contrast, is dominated by the transverse optic (TO) vibration modes of phonons centered at 114 cm^{-1} [86], which is consistent with the presence of CuI–containing phase. However, definitive crystallographic confirmation would require XRD analysis. No Raman features assignable to copper oxides can be detected, indicating that no significant oxidation occurred during particle preparation.

When particles are mixed in the sol–gel matrix, the spectra of the 2.04 wt% and 4.08 wt% composites retain the stretching bands between 2887 and 2926 cm^{-1} arising from the aliphatic groups of polyvinyl alcohol and characteristic of the pristine xerogel, demonstrating that incorporation of CuI–PVA does not disrupt the siloxane backbone. At the same time, the 114 cm^{-1} mode ascribed to Cu–I vibrations re-emerges, and its intensity increases proportionally with the particle loading, providing direct spectroscopic evidence that CuI survives the acidic sol–gel environment and remains Raman-active within the hybrid network. The –CH_2 stretching band likewise grows with higher CuI–PVA content, reflecting the increasing amount of organic polymer.

Raman data confirm the coexistence of an intact siloxane scaffold and unaltered CuI particles stabilized by PVA. The absence of new bands related to copper oxides or metallic copper excludes unwanted side reactions, while the progressive rise of PVA-derived vibrations indicates that the organic fraction, and therefore the flexibility and adhesion of the coating, can be tuned without compromising structural integrity. Overall, these spectroscopic findings support the formation of a hybrid CuI–PVA/siloxane network in the xerogel, providing a structural basis for the coating system further investigated on cotton fabrics in terms of surface retention and antibacterial performance after laundering.

3.2.3. DLS and zeta potential measurements of sol–gel dispersed CuI–PVA particles

Fig. 5a and 5b illustrate the hydrodynamic size distributions of

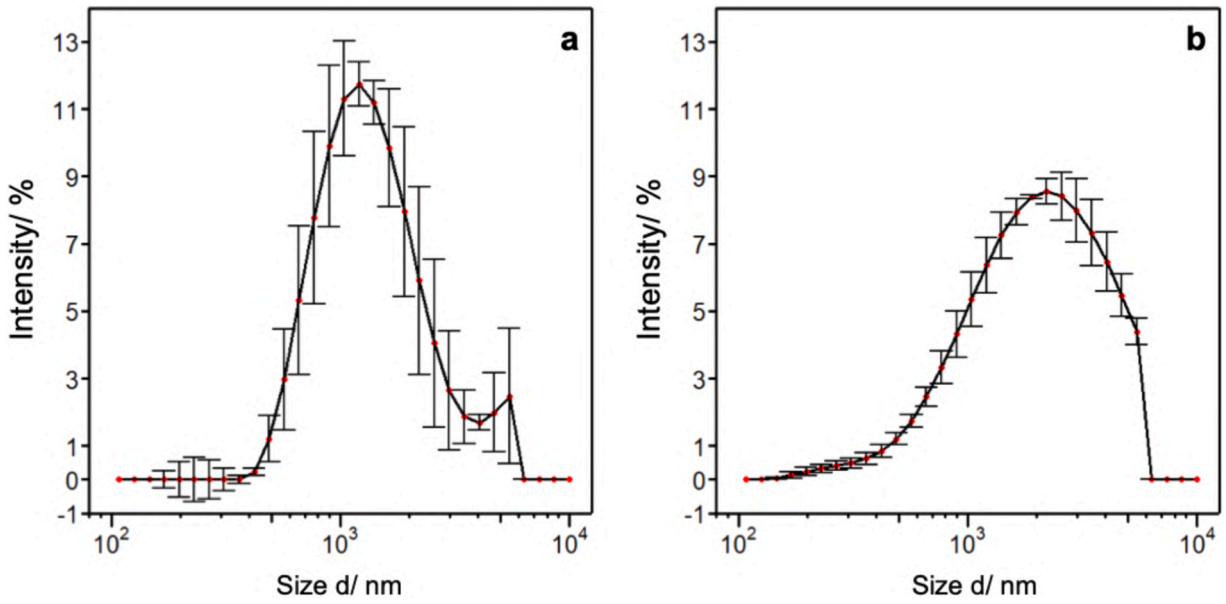

Fig. 5. Particle size distribution curves of sol–gel dispersed CuI–PVA micrometer-scale clusters at 2.04 wt% (a) and 4.08 wt% (b).

CuI–PVA particles dispersed in sol–gel matrices at two concentrations, 2.04 wt% and 4.08 wt%, respectively, as determined by dynamic light scattering (DLS). Both samples exhibit broad, polydisperse distributions, with hydrodynamic diameters ranging from approximately 420 nm to 5500 nm for the 2.04 wt% sample and from 150 nm to 5500 nm for the 4.08 wt% formulation.

The silane-based formulation containing 2.04 wt% of CuI–PVA (Fig. 5a) exhibits a multimodal profile: i) no particle population is detected below 400 nm, suggesting either the absence or weak scattering contribution of smaller species; ii) a dominant size population is centered around 1209 nm, with an intensity maximum of 11.7%, accompanied by neighboring contributions at 1039 nm (11.3% of total intensity) and 1406 nm (11.2% of total intensity) indicating partial aggregation or polydisperse clustering; iii) a secondary broad signal appears at 5468 nm (2.5% of total intensity), consistent with the formation of larger micrometer-scale aggregates. These features suggest that at lower CuI–PVA concentrations, particles tend to form loose clusters due to limited steric stabilization within the silane matrix.

Conversely, the sol–gel CuI–PVA 4% (Fig. 5b) exhibits a broader and nearly monomodal particle distribution, starting from approximately 146 nm and peaking at 2211 nm (8.5%). The intensity rises gradually across the submicron range and decreases gently above 2500 nm, without displaying distinct secondary peaks. This behavior suggests that higher CuI–PVA loading promotes more effective dispersion within the sol–gel network; increased interparticle interactions under these conditions favor the formation of a more uniform, submicron-dominated distribution.

Both SEM and DLS results indicate that the CuI–PVA phase is present as submicrometric-to-micrometric particulate aggregates/particles rather than unequivocally nanosized isolated ones. As a matter of fact, SEM provides the morphology of the dried CuI–PVA compact aggregates/particles after solvent evaporation and eventually aggregation phenomena, which are predominantly submicrometric and generally range from a few hundred nanometers to about 1 μm, with occasional larger coalesced aggregates. On the other hand, DLS measures the hydrodynamic diameter of the dispersed species in the liquid sol–gel medium; this value includes not only the inorganic core, but also the capping PVA layer together with the interpenetrating solvent molecules, i.e., without interparticle association phenomena observed by SEM images. Consequently, the DLS distributions are broader and shifted toward larger apparent sizes, with dominant populations centered at 1039–1406 nm for the 2.04 wt% formulation and at 2211 nm for the 4.08 wt% formulation, together with contributions from larger aggregates. The apparent discrepancy between SEM and DLS is therefore expected and reflects the difference between the dry-state morphology and the hydrodynamic behavior of dispersed CuI–PVA aggregates/particles [87].

Both GT CuI–PVA 2.04 wt% and 4.08 wt% samples exhibit high polydispersity indices (PDI of 0.3018 ± 0.04456 and 0.3376 ± 0.01694, respectively), confirming broad size distributions. At the lower loading (2.04 wt%), the DLS profile reveals micrometer-scale clusters which reduce the effective interfacial area available for particle–matrix interactions and can act as stress-concentrating defects, thereby compromising the mechanical integrity of the hybrid coating. At higher loading (4.08 wt%), although monodispersity is not achieved, the distribution shifts toward a more uniform submicron–to–low-micron regime, with fewer large aggregates.

These findings underscore the pivotal role of CuI–PVA concentration in governing colloidal stability and aggregate formation within sol–gel matrices.

Zeta potential measurements were carried out to assess the surface charge characteristics of CuI–PVA particles embedded within sol–gel matrices and their implications for colloidal stability and interfacial interactions. The measured zeta potentials were -16.56 ± 0.5254 mV for the 2.04 wt% sample and -16.55 ± 0.8094 mV for the 4.08 wt% formulation. These slightly negative surface potentials suggest limited electrostatic repulsion between particles, which, although not sufficient for full colloidal stabilization, may improve dispersion stability when combined with steric hindrance from the PVA polymer chains. Furthermore, the overall negative surface charge may influence interactions with bacterial membranes, which are also typically negatively charged, potentially affecting antibacterial activity through indirect mechanisms such as membrane perturbation or interference with surface-bound enzymes.

3.3. Characterization of cotton fabrics treated with CuI–PVA-based sol–gel finishing

3.3.1. Functionalization of cotton fabrics and physicochemical characterization

Table S1 in Supplementary Material summarizes the liquor retention (wet pick-up) recorded during the pad–dry–cure step and the final mass

gain (add-on) of the finished cotton fabrics. The reference sol–gel formulation (CO_GT) yields a wet pick-up of 74.6%, consistent with the uptake typically observed for low-viscosity silane solutions on medium-weight woven cotton. Replacing part of the liquid phase with the CuI–PVA dispersion slightly increased liquor retention to 82.3% and 82.4% for the 2.04 wt% and 4.08 wt% formulations, respectively. The near-constant values indicate that the presence of the sol phase does not substantially alter bath rheology, so the padding parameters remain unchanged.

The corresponding add-on values increase almost proportionally with the CuI–PVA content. While the plain GPTMS–TEOS coating contributes a mass increment of 1.17%, introducing 2.04 wt% CuI–PVA nearly doubles the add-on to 1.98%, and 4.08 wt% CuI–PVA increases it to 2.57%. These figures confirm that the CuI–PVA particles are efficiently transferred from the bath to the substrate and retained during drying and curing. Notably, even the highest add-on remained below 3%, indicating that the functional phase was deposited at a relatively low mass loading. However, the influence of the coating on fabric flexural behavior was further assessed through bending stiffness measurements, while dedicated future measurements will be achieved to assess handle, breathability, or comfort-related properties. Nevertheless, the wet-pick-up and add-on data therefore demonstrate that the hybrid CuI–PVA/siloxane finish can be applied using standard padding equipment, providing predictable loading of the functional species, and suggesting its potential for industrial upscaling.

Cellulose, the main component of cotton, is a carbohydrate polymer comprising repeating β-D-glucopyranose units covalently linked through acetal bonds between the equatorial hydroxyl group at C1 and the C4 carbon atoms. Its linear structure features three hydroxyl groups per anhydroglucose unit, which contribute to hydrogen bonding, influencing the material's reactivity and interaction with functional coatings. In this study, cotton samples were coated with a hybrid tetraethoxysilane (TEOS), and (3-Glycidyloxypropyl)trimethoxysilane (GPTMS) sol–gel solution containing CuI nanostructured particles capped with PVA. The hydrolysis and condensation reactions of these silicon alkoxides, conducted at relatively low temperature under soft-chemistry conditions, led to the formation of an amorphous three-dimensional silicon oxide network [88].

The silicon-based matrix was introduced not to generate antibacterial activity per se, but to serve as a carrier and fixation phase for the CuI–PVA component during textile finishing. Upon hydrolysis and condensation of TEOS and GPTMS, a siloxane-rich network is formed on the hydroxyl-rich cotton surface, enabling the formation of a continuous coating through a conventional pad–dry–cure process. In this hybrid system, the matrix fulfills several functions: it provides structural cohesion to the deposited layer, improves interfacial compatibility between the cotton substrate and the PVA-stabilized CuI phase, favors a more homogeneous distribution of the copper-containing particles, and helps reduce their loss during rinsing and laundering. GPTMS is particularly important in this context because its organofunctional character contributes to balancing the rigidity of the inorganic siloxane framework with the flexibility and adhesion required for textile applications. Therefore, the silicon-based matrix is necessary from a technological standpoint, since it acts as a coupling/binding layer for nanoparticle fixation and washing durability, consistent with previous studies on functional cotton finishing using silane coupling agents [9]. When applied to cotton surfaces, the hydrolyzed GPTMS–TEOS sol is expected to form a siloxane-rich hybrid network that adheres to the hydroxyl-rich cellulose surface through a combination of silanol condensation, hydrogen bonding, and interfacial compatibility effects typical of alkoxysilane-based systems. GPTMS is also expected to improve compatibility with the PVA-stabilized CuI phase through its organofunctional glycidoxypropyl moiety. However, because the ATR-FTIR region associated with possible Si–O–C contributions overlaps strongly with intense cellulose and siloxane absorptions, the present data do not provide direct proof of specific fiber–O–Si covalent linkages in this system. The interfacial bonding is therefore discussed here as chemically plausible and consistent with established silane chemistry, rather than as spectroscopically demonstrated.

The FTIR spectrum of untreated cotton (Fig. 6, black curve) displays characteristic absorption bands in the range 3500–3100 cm^{-1}, 3000–2800 cm^{-1}, and 1200–800 cm^{-1}, corresponding to the stretching vibrations of the –OH, C–H, and C–O–C glycosidic bonds, respectively.

The ATR-FTIR spectra of untreated and treated cotton fabrics are largely superimposable, which is expected considering that the deposited hybrid layer is relatively thin and that the infrared response is dominated by the cellulose substrate. Under these conditions, the spectral contributions of the GPTMS/TEOS-derived coating and of the CuI–PVA phase are necessarily weak and partly overlapped by the intense absorption bands of cotton.

Nevertheless, some modest but reproducible variations can be observed after treatment. In particular, the broad O–H stretching envelope in the 3500–3000 cm^{-1} region becomes slightly less intense and somewhat broader in the coated samples, which is consistent with a modified hydrogen-bonding environment at the fiber surface after deposition of the hybrid layer. In addition, minor changes are observed in the 1200–1000 cm^{-1} region, where the characteristic cellulose vibrations overlap with possible Si–O–Si and Si–O–C contributions from the sol–gel network.

However, owing to the strong spectral contribution of cellulose and the relatively low add-on of the coating, the ATR-FTIR data do not allow an unambiguous assignment of all interfacial bonds, nor do they show intense new bands uniquely attributable to the siloxane network. Therefore, ATR-FTIR should be regarded here as providing evidence consistent with surface functionalization, rather than definitive proof of specific bonding formation taken in isolation. The occurrence of the coating and its persistence on the cotton surface are more convincingly supported by the combined spectroscopic and microscopic evidence, particularly Raman spectroscopy and SEM-EDS.

Raman spectra in Fig. 7 compare the vibrational fingerprints of pristine cotton (CO_UT, black), cotton finished with the GPTMS–TEOS matrix alone (CO_GT, red), and cotton fabric functionalized with the same matrix carrying 2.04 wt% and 4.08 wt% CuI–PVA nanostructured particles (green and blue, respectively).

The untreated fabric displays the expected characteristic vibrational bands of a cellulose-based material. The peak at 377 cm^{-1} can be attributed to C–C–C ring deformations, while the sharp band at 1093 cm^{-1} is related to the asymmetric stretching vibrations of the C–O–C glycosidic bonds. Moreover, the set of bands at 1293, 1336, and 1373 cm^{-1} reflects various CH_2 and CH bending modes of the glucopyranose backbone [67]. The intense line at 2896 cm^{-1} corresponds to symmetric C–H stretching, and the broad band centered at 3292–3368 cm^{-1} is due to hydrogen-bonded O–H stretching; a weak, low-intensity band between 1630 and 1740 cm^{-1} is attributable to adsorbed water or minor carbonyl groups produced by natural oxidation of the fibers [89].

After deposition of the GPTMS–TEOS sol–gel layer, the cellulose bands remain visible, but their relative intensities diminish, consistent with partial masking of the underlying substrate by a silica-rich overlayer. No additional Raman modes diagnostic of crystalline silica can be detected, as expected for an amorphous siloxane network.

The introduction of CuI–PVA clusters resulted in two notable changes. First, the low-wavenumber region exhibits additional bands at approximately 336, 377, and 439 cm^{-1}, which are consistent with vibrations associated with the copper-containing inorganic phase [90]. Together with the SEM-EDS detection of Cu and I, these features support the presence of a CuI-containing phase on the textile substrate after the pad–dry–cure treatment. In the absence of XRD, however, this assignment should be regarded as supportive rather than definitive from a crystallographic standpoint. Second, a broad band appears in the 1630–1740 cm^{-1} region, indicating new carbonyl-type vibrations that can be ascribed to interaction with silanol groups engaged in hydrogen bonding. Moreover, the band centered at 3292–3368 cm^{-1} increases in

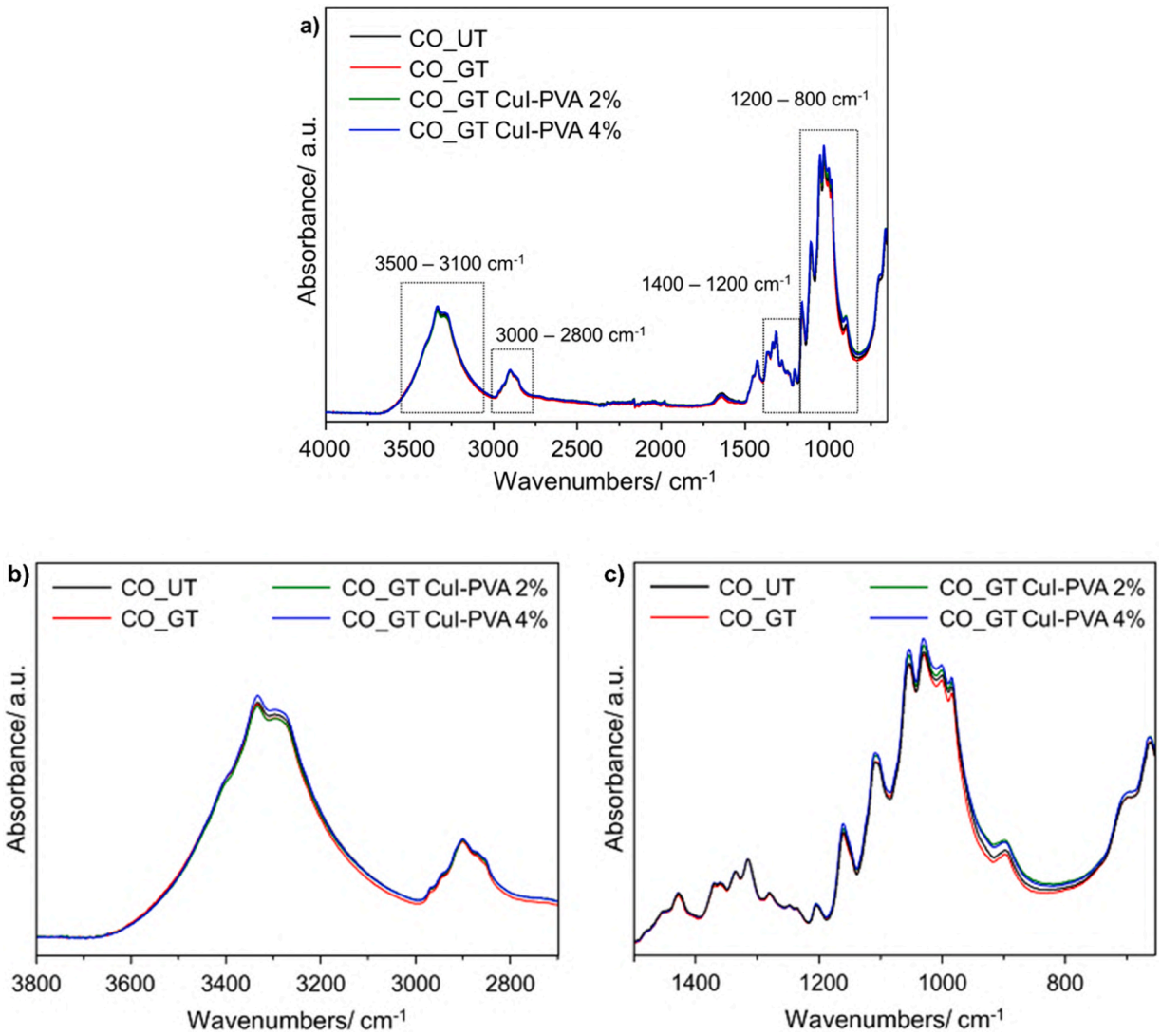

Fig. 6. ATR-FTIR spectra of untreated cotton (black curve) and cotton treated with GPTMS–TEOS sol–gel (red curve) and GPTMS–TEOS sol embedding CuI–PVA at 2.04 wt% and 4.08 wt% (green and blue curves, respectively). The spectra are shown in selected wavenumber regions where the most pronounced differences are observed.

intensity, reflecting stronger hydrogen-bonding interactions among silanols, PVA hydroxyls, and the surface hydroxyl groups of cotton. These interactions are likely to enhance coating adhesion and explain the observed washing fastness of the functionalized fabrics [91]. Notably, the cellulose backbone retains its characteristic 1093 cm^{-1} signature in all spectra, ruling out bulk degradation of the fibers during the sol–gel and nanostructure treatments.

Together with the SEM-EDS evidence of Cu and I, these Raman features support the presence of a CuI-containing phase on the textile substrate after the pad–dry–cure treatment. Similar application-oriented characterization strategies based primarily on microscopy/spectroscopy and functional evidence, rather than on diffraction as the central tool, have also been reported in the literature for copper-based antimicrobial materials and coatings [9,38]. However, in the absence of XRD data, the present assignment should be considered supportive rather than definitive from a crystallographic standpoint. Full phase confirmation of the inorganic component would require XRD analysis.

3.3.2. *Surface morphology*

Fig. 8 presents SEM images of the uncoated and coated textile samples. The pristine cotton fabric (Fig. 8a–c) displays a clean, uncoated surface, whereas the 2.04 wt% and 4.08 wt% CuI–PVA-coated samples (Fig. 8i–k and 8m–o, respectively) exhibit a distinct polymeric film on the fiber surface, acting as an effective medium for bonding and securing the particles to the substrate. SEM-EDS micrographs of the functionalized samples (Fig. 8l and 8p) confirm the deposition of the coating and the incorporation of CuI within the sol–gel matrix. As shown in Fig. 8j and 8n, the copper-containing coating fully envelops the textile fibers, creating a uniform layer with an increased surface roughness. The primary structure consists of sparsely distributed CuI–PVA particulate domains embedded within a highly interconnected network. At higher magnifications (Fig. 8k and 8o), a homogeneous, integrated microstructure is evident, indicating a relatively uniform distribution of the CuI–PVA particulate phase within the coating. These results suggest that the proposed method effectively disperses the Cu-containing particles, even after drying, by mitigating their natural tendency to agglomerate because of their high surface energy. EDS elemental analysis and mapping further confirmed the presence and distribution of Si and Cu across all coatings, supporting the effective deposition of the hybrid finish on the cotton surface.

3.3.3. *Thermal characterization*

In Fig. 9, the thermogravimetric curves of pristine cotton (CO_UT) and cotton finished with the GPTMS/TEOS matrix, either neat (CO_GT)

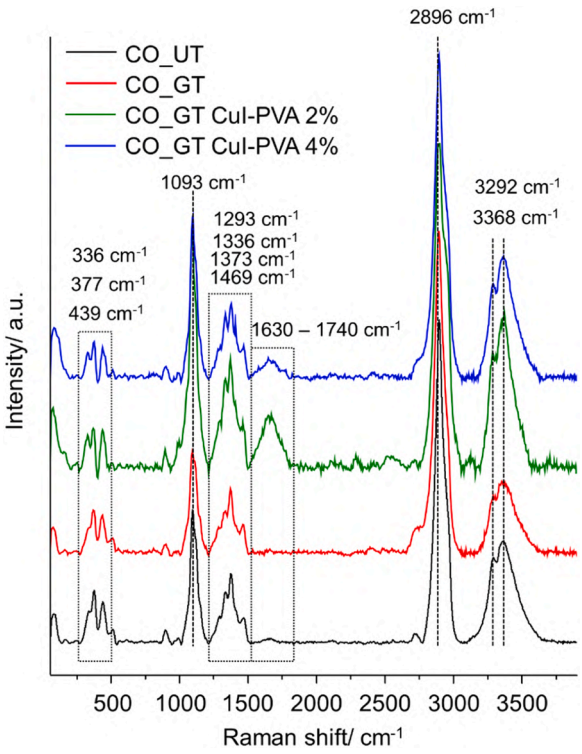

Fig. 7. Raman spectra of untreated cotton (black curve) and cotton treated with GPTMS–TEOS sol–gel (red curve) and GPTMS–TEOS sol embedding CuI–PVA nanostructured particles at 2.04 wt% and 4.08 wt% (green and blue curves, respectively).

or loaded with 2 wt% and 4 wt% CuI–PVA nanostructured particles (CO_GT CuI–PVA 2% and CO_GT CuI–PVA 4%), reveal the typical two-stage degradation pattern of cellulosic fibers. All specimens display a minor mass loss below 120°C, attributable to the desorption of physically bound water, followed by an abrupt drop that begins at approximately 305–310°C and reaches its maximum rate near 340–345°C, corresponding to the depolymerization of the glucopyranose backbone and volatilization of levoglucosan. The coincidence of both the onset and the peak temperatures for all four curves demonstrates that neither the siloxane network nor the CuI–PVA nanostructured particle catalyzes premature thermal degradation; therefore, the thermal stability window of the treated fabrics remains comparable to that of the untreated substrate.

Beyond 380°C, the untreated sample continues to lose mass and levels off at approximately 4%–5% residue at 700°C, whereas the finished fabrics retain progressively larger residues, approximately 7% for CO_GT, 9% for the 2.04 wt% composite and 11% for the 4.08 wt% composite. This incremental gain is consistent with the inorganic fraction of the coating (silica from the GPTMS–TEOS condensation and CuI), confirming the presence of the finish without altering the course of cellulose oxidative degradation. No additional low-temperature events or shoulders can be detected, indicating that the organic components of the sol–gel layer (opened GPTMS epoxides and PVA chains) are either tightly integrated into the silica framework or present in amounts too small to generate separate degradation steps.

The TGA results demonstrate that the hybrid CuI–PVA/siloxane finishing leaves the intrinsic thermal behavior of cotton essentially unchanged, while introducing an inorganic residue that may confer a slight char-forming benefit at high temperatures. These findings are consistent with earlier reports on silica-based textile coatings and confirm that the current treatment is suitable for applications requiring steam sterilization or other thermal stresses where maintaining the fabric's integrity is essential.

3.4. Antibacterial performance of CuI-based hybrid finishes

Antimicrobial treatments are crucial for protecting cotton textiles against biodeterioration, limiting pathogen transmission, and reducing the attendant odors, dermatitis, and other health issues that arise from microbial colonization. In the present work, the antibacterial efficacy of the hybrid GPTMS/TEOS–CuI–PVA finish was quantified against *S. aureus* and *E. coli* according to the reduction factors listed in Table 1 (codes: CO_UT = untreated cotton, CO_GT = siloxane matrix only, CO_GT CuI–PVA 2% and CO_GT CuI–PVA 4% = hybrid coatings with 2.04 wt% and 4.08 wt% nanostructured particles, respectively).

The antibacterial activity of the CuI–PVA/siloxane coatings is discussed here in the light of mechanisms reported for copper-based antimicrobial materials, rather than as a directly demonstrated nanoenzyme-like pathway in the present system. Copper species associated with the coating may interact with negatively charged bacterial envelopes, thereby promoting membrane destabilization and contributing to oxidative stress and intracellular damage [77]. Based on previous literature on CuI- and copper-based antibacterial systems, ROS generation through redox cycling may also be proposed as a possible pathway contributing to the observed antibacterial response. Under aerobic conditions, when the CuI–PVA phase comes into contact with bacterial cells, a generic antioxidant substrate (AH_2) present in the biological environment may first undergo oxidation, leading to the formation of hydrogen peroxide (H_2O_2) (Eq. 10). Subsequently, the CuI–PVA surface may promote H_2O_2 decomposition, generating highly reactive hydroxyl radicals (•OH) (Eq. 11) [92].

$$AH_2 + O_2 \longrightarrow A + H_2O_2 \text{ (oxidase-like step)} \quad (10)$$

$$H_2O_2 + Cu^{+} \longrightarrow \bullet OH + OH^{-} + Cu^{2+} \text{ (peroxidase-like step)} \quad (11)$$

These reactive oxygen species could contribute to bacterial inactivation by inducing oxidative damage to cell membranes, proteins, and nucleic acids. However, since ROS-specific assays were not performed in the present study, the relative contribution of this pathway remains to be established.

Both reference materials, CO_UT and CO_GT, supported unhindered growth of the two bacterial strains, confirming the absence of intrinsic biocidal activity in pristine cotton and in the neat siloxane network. In contrast, the CuI-finished fabrics achieved an initial bacterial reduction of 99.5 ± 0.07% (*S. aureus*) and 99.1 ± 0.08% (*E. coli*) for the 2 wt% formulation and 99.2 ± 1.20% (*S. aureus*) and 99.0 ± 0.65% (*E. coli*) for the 4 wt% formulation. After one ISO 105-C10 laundering cycle, reductions remained above 99% for both organisms and both loadings and were essentially retained after three cycles (≥ 99.5% for *S. aureus* and 98.7 ± 1.84% for *E. coli* at the highest loading). The antibacterial performance observed here is consistent with previous reports on copper-functionalized cotton, where high activity has been achieved with CuO- and Cu_2O-based systems [9,34].

The antimicrobial action may involve copper species associated with the embedded CuI–PVA phase. Owing to the negative charge of bacterial cell envelopes, Cu^{+}/Cu^{2+} ions are electrostatically attracted to these surfaces, where they can be adsorbed and promote membrane destabilization and permeability changes, thereby facilitating subsequent cellular uptake.

According to mechanisms widely reported for copper-based antimicrobials, once copper species gain access to the cell, they may interact with thiol-containing residues, impair essential metabolic enzymes, promote the formation of reactive oxygen species (ROS) through redox cycling, and perturb nucleic-acid processes, collectively leading to irreversible loss of cellular function and cell death [21]. While the antibacterial behavior of CuI–PVA coatings is consistent with peroxidase-like catalytic pathways, this mechanism has not yet been experimentally verified. Further investigations, including reactive oxygen species detection or H_2O_2 consumption assays, will be conducted to confirm the catalytic contribution of Cu^{+}/Cu^{2+} redox cycles to the

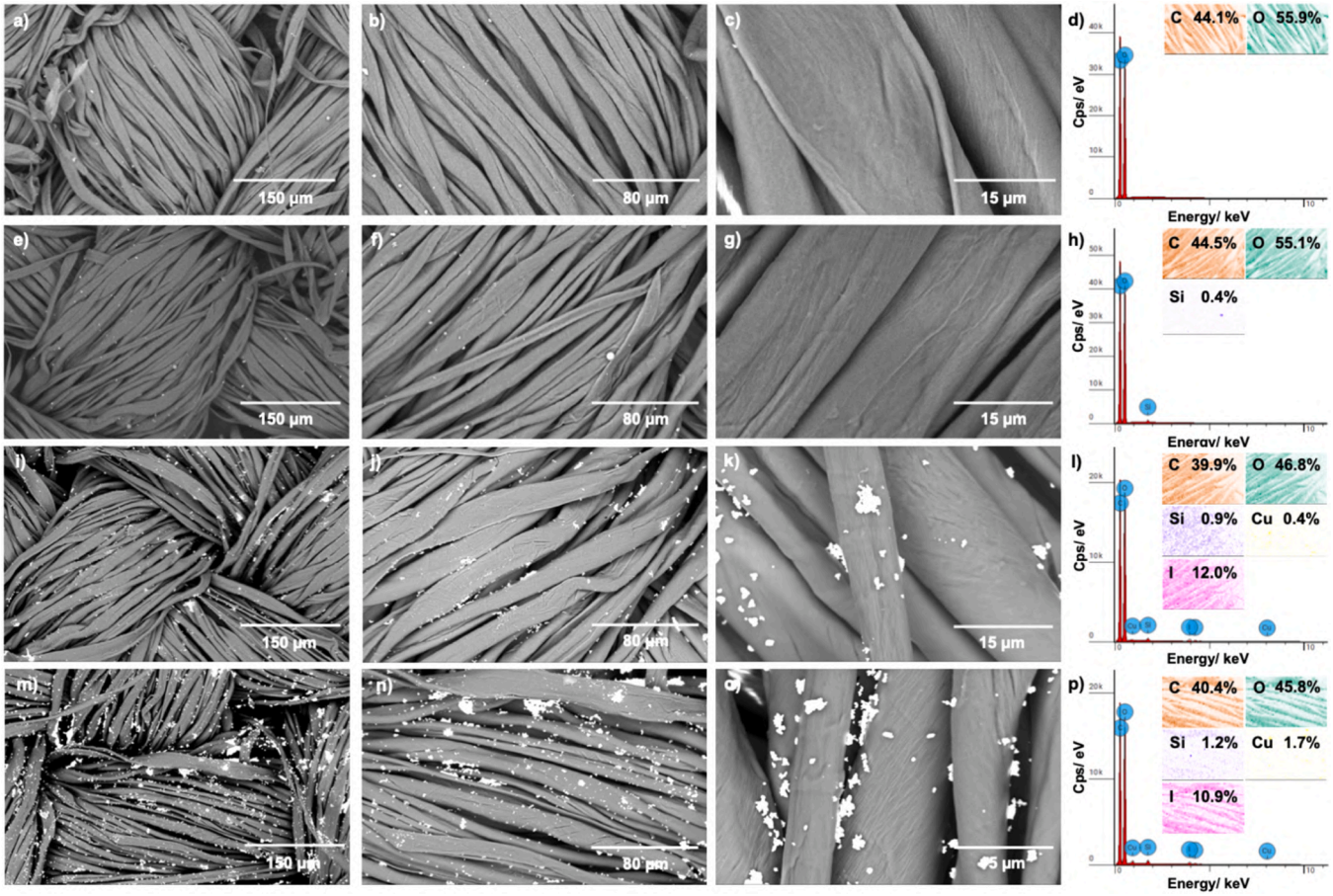

Fig. 8. SEM and EDS characterization of untreated cotton (a–d), sol–gel treated cotton (e–h), GT CuI–PVA 2% treated cotton (i–l), and GT CuI–PVA 4% treated cotton fabrics (m–p). The EDS results are reported as elemental analysis/mapping for improved readability, while the corresponding enlarged spectra are provided in the Supplementary Material (Fig. S2).

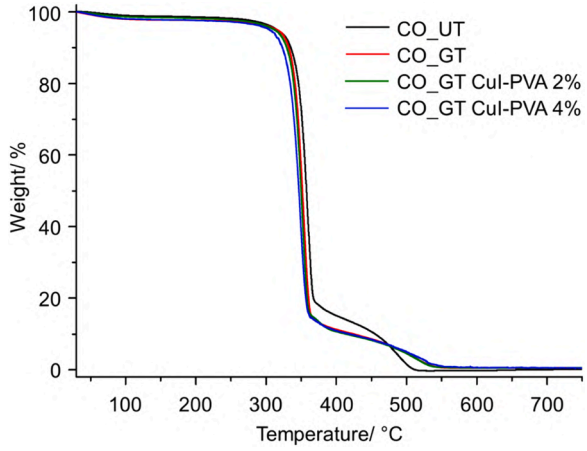

Fig. 9. TGA curves of cotton fabrics, both untreated and treated with silane-based CuI–PVA.

Table 1
Bacterial reduction (%) of untreated and treated fabrics against *S. aureus* and *E. coli*, also after 1 and 3 washing cycles. Results are reported as mean ± standard deviations of data obtained from triplicate experiments, with independent microbial cultures for each antimicrobial assay. No statistically significant differences were detected among the CuI–PVA-treated samples and washing conditions at the 5% significance level.

Cotton sample	Bacterial reduction (%)					
	UW		1W		3W	
	S. aureus	*E. coli*	*S. aureus*	*E. coli*	*S. aureus*	*E. coli*
CO_UT	0	0	/	/	/	/
CO_GT	0	0	/	/	/	/
CO_GT CuI–PVA 2%	99.5 ± 0.07	99.1 ± 0.08	99.4 ± 0.07	99.5 ± 0.36	100.0 ± 0.0	99.5 ± 0.02
CO_GT CuI–PVA 4%	99.2 ± 1.20	99.0 ± 0.65	100.0 ± 0.0	99.5 ± 0.02	100.0 ± 0.0	98.7 ± 1.84

observed antibacterial activity. In addition, X-ray photoelectron spectroscopy (XPS) to determine the oxidation state and local chemical environment of copper in the CuI–PVA–siloxane matrix before and after laundering will be performed with the aim of providing quantitative insight into Cu^{+}/Cu^{2+} ratios and validating the proposed redox-driven antibacterial mechanism. Moreover, this first-stage study did not include cytotoxicity or skin-compatibility tests of the CuI–PVA finishing on mammalian cells. These experiments are planned as a second step in the research to fully assess the safety of the treated textiles. Nevertheless, existing literature suggests that CuI-based coatings and copper-containing nanomaterials can achieve strong antibacterial effects within acceptable biocompatibility windows when properly formulated and dosed. For example, Chen et al. [93] reported that cotton fabrics coated in situ with CuI nanoparticles showed broad-spectrum antimicrobial activity, while extracts of the coated fabrics maintained high viability of L929 fibroblasts and did not cause detectable histopathological alterations in a mouse skin contact model, suggesting

acceptable skin tolerance under the specific tested conditions and supporting their potential suitability for direct skin-contact applications.

In a complementary approach, Hernandez et al. [94] evaluated CuI and TiO_2–Cu^{2+}/CuI nanocomposites and found dose-dependent effects on human bronchial epithelial BEAS-2B cells: cell viability remained relatively high at low surface doses but decreased at 2.5–5.0 $\mu g \cdot cm^{-2}$ after 24 h, indicating that these materials are biocompatible only within a certain concentration range. Reviews of copper-containing nanoparticles in biomedical contexts similarly conclude that, when incorporated at appropriate levels into coatings or composites, copper-based systems can combine potent antimicrobial activity with limited cytotoxicity, although high doses or prolonged exposure can lead to inflammation, oxidative stress, and tissue damage [95,96]. Moreover, intentional use of CuI nanoparticles as anticancer agents has shown clear, dose-dependent cytotoxicity in tumour cell lines, underscoring that biological responses to CuI are strongly dependent on dose, exposure conditions, and cell type [97]. Overall, these findings support the feasibility of developing safe CuI-based antibacterial finishes for cotton, while also reinforcing the need for dedicated cytotoxicity and irritation studies in future work for the specific CuI–PVA sol–gel system presented here.

The GPTMS–TEOS siloxane scaffold appears to act as a carrier and fixation matrix for the PVA-stabilized CuI phase, supporting its retention on the cotton surface under the tested laundering conditions. The proposed coatings rely on the inherent compatibility between the inorganic CuI core, the hydrophilic PVA corona, and the flexible siloxane network. The retained antibacterial activity after the tested washing cycles suggests that this organic–inorganic structure maintains an unobstructed diffusion pathway for copper ions, thereby inferring that a sufficient amount of the active CuI–PVA phase remains available at the textile surface. Collectively, the results support the GPTMS–TEOS CuI–PVA finish as an effective proof-of-concept antibacterial treatment for cotton fabrics, with activity retained after three ISO 105-C10 washing cycles.

3.5. Textile properties

The influence of the CuI–PVA/siloxane coatings on the textile properties of cotton fabrics was evaluated in terms of bending stiffness. This assessment is particularly relevant because functional finishing treatments, although effective in imparting antibacterial activity, may modify the mechanical response and comfort-related behavior of textile substrates. The immobilization of inorganic particles generally requires a binding or coupling matrix to improve adhesion and washing durability; however, the presence of an additional coating layer and dispersed particulate domains may affect fabric handle, flexibility, and drape. Therefore, the preservation of textile softness after finishing represents an important requirement for practical applications, especially in hygienic, medical, and technical textiles.

In the present study, textile stiffness was assessed for untreated cotton (CO_UT), cotton treated with the GPTMS–TEOS sol–gel matrix alone (CO_GT), and cotton functionalized with the hybrid CuI–PVA/siloxane formulations containing 2.04 wt% and 4.08 wt% CuI–PVA (CO_GT CuI–PVA 2% and CO_GT CuI–PVA 4%, respectively) (Table 2).

The untreated cotton fabric showed a bending stiffness value of 12.1 ± 0.4 $cN \cdot cm^2$. After application of the unloaded GPTMS–TEOS matrix, the value increased slightly to 12.9 ± 0.5 $cN \cdot cm^2$, indicating only a limited change in the flexural behavior of the fabric. This variation can be attributed to the formation of a thin siloxane-based network on the fiber surface, which acts as a cohesive coating without completely masking the inherent flexibility of the cellulose substrate.

Table 2
Bending stiffness (B) calculated according to DIN 53362 for untreated, sol-gel treated and CuI–PVA/siloxane treated cotton.

Sample	Bending Stiffness ($cN \cdot cm^2$)
CO_UT	12.1 ± 0.4
CO_GT	12.9 ± 0.5
CO_GT CuI–PVA 2%	13.3 ± 0.4
CO_GT CuI–PVA 4%	13.5 ± 0.5

The incorporation of CuI–PVA particles within the GPTMS–TEOS matrix resulted in bending stiffness values of 13.3 ± 0.4 $cN \cdot cm^2$ for CO_GT CuI–PVA 2% and 13.5 ± 0.5 $cN \cdot cm^2$ for CO_GT CuI–PVA 4%. The observed trend suggests that the CuI–PVA loading does not substantially affect fabric stiffness compared with the neat sol–gel treatment. The slight increase in bending stiffness may be attributed to CuI–PVA particulate domains embedded within the hybrid siloxane network, which can increase the rigidity of the deposited layer with increasing particle content. At the same time, the PVA component and the organofunctional GPTMS-derived segments may contribute to maintaining interfacial flexibility, limiting excessive stiffening of the cotton fabric.

Overall, the bending stiffness results indicate that the hybrid CuI–PVA/siloxane finishing can be applied to cotton, suggesting only a slight increase in stiffening under the tested conditions, as a first handle-related indication. This finding is consistent with the intended role of the GPTMS–TEOS matrix, which provides coating cohesion and particle anchoring while avoiding the formation of an excessively rigid continuous layer. These data should not be extrapolated to tensile strength, elongation at break, air permeability, or water-vapor transmission, which require dedicated testing and remain outside the scope of the present study. However, the balance between antibacterial functionality, coating durability, and limited alteration of bending behavior supports the potential use of these CuI–PVA-based finishes for cotton fabrics intended for repeated-use hygienic and technical applications.

3.6. Durability of copper-based sol–gel finishing

In the present study, retention of antibacterial function after laundering is established only by the microbiological results reported in Table 1, whereas SEM-EDS and ATR-FTIR are discussed solely as complementary evidence of coating persistence on the fiber surface. Table S2 in the Supplementary Material demonstrates that the hybrid CuI–PVA/siloxane coatings withstand domestic laundering with minimal material loss. The GPTMS–TEOS matrix alone (CO_GT) shows a 1.17% weight reduction after the first wash and 0.65% reduction after three washes; these values reflect the removal of weakly bound siloxane fragments that are typically present on freshly cured films.

The addition of the CuI–PVA particles significantly enhances wash fastness. At 2.04 wt% loading, weight loss decreases to 0.71% after the first wash, with no additional loss observed after two further washes (0.66%). At 4.08 wt%, the finish becomes essentially highly stable: weight loss is limited to 0.24% after one wash, reducing further to a negligible 0.09% after three cycles. This trend suggests that the hydroxyl-rich PVA corona surrounding the CuI particles forms extra hydrogen bonds with residual silanols in the matrix and the cellulosic surface, thereby strengthening the interphase and preventing elution.

All coatings remain well below the 3% residual mass loss threshold, which is generally regarded as the upper limit for commercially durable textile finishes. This finding suggests good retention of the hybrid CuI–PVA finish under the tested laundering conditions, although its suitability for repeated use in healthcare and consumer applications requires confirmation through future long-term washing durability, post-wash antibacterial, mechanical, and comfort-related assessments.

SEM images in Fig. 10 confirm that the hybrid CuI–PVA/siloxane coating is still present on the cotton surface after laundering, although they also indicate some local morphological rearrangement of the outermost deposited layer. In the 2.04 wt% formulation, before washing (Fig. 10a–d), the CuI–PVA phase appears as particulate deposits distributed along the fiber surface and natural yarn grooves. The corresponding EDS elemental analysis (panel d) confirms the presence of silicon (≈ 0.9 wt%) from the siloxane matrix and copper (≈ 0.4 wt%) from the CuI-containing phase. After one (Fig. 10e–h) and three

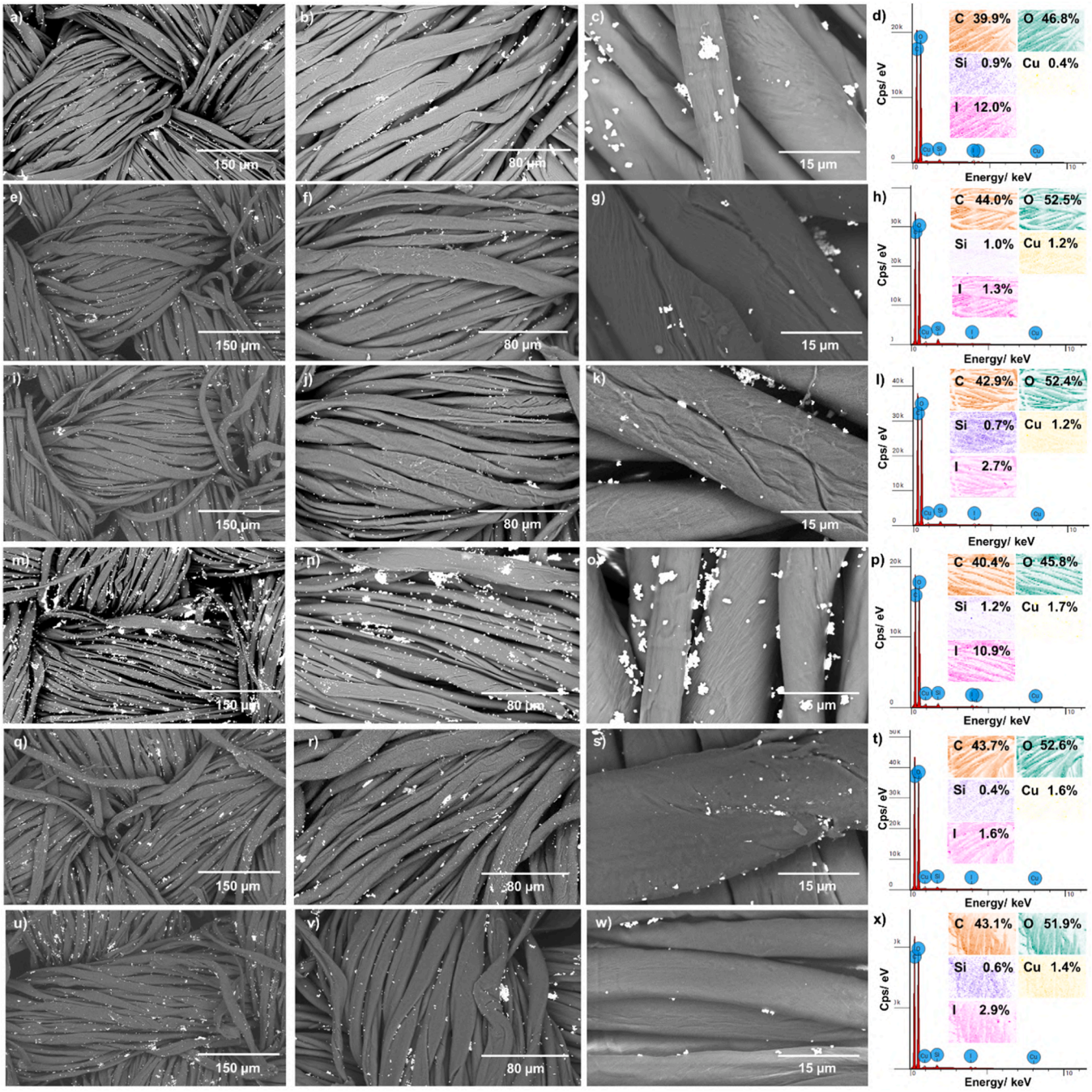

Fig. 10. SEM and EDS characterization of CO_GT CuI–PVA 2% (a–d) before washing and after 1 (e–h) and 3 (i–l) washing cycles; CO_GT CuI–PVA 4% (m–p) before washing and after 1 (q–t) and 3 (u–x) washing cycles. The EDS data are shown as elemental analysis/mapping for clearer visualization; the corresponding enlarged spectra are reported in the Supplementary Material (Fig. S3).

(Fig. 10i–l) ISO 105-C10 washing cycles, Si and Cu are still detected by EDS, confirming persistence of the coating; however, the surface appears locally smoother and less particulate in some regions, which is more appropriately interpreted as partial redistribution, compaction, or removal of loosely bound superficial material, rather than complete morphological invariance. A similar behavior is observed for the 4.08 wt % formulation (Fig. 10m–x), where the initially higher surface coverage is substantially retained after washing, although some local heterogeneity remains visible [2].

These SEM observations are not necessarily inconsistent with the very low WLW% values reported in Table S2. Indeed, WLW% represents the average gravimetric mass loss of the whole fabric specimen, whereas SEM examines only selected microscopic surface areas. Consequently, limited local topographical changes may occur even when the total coating mass loss remains very small. In the same way, the fluctuations observed in the EDS Cu signal after washing should be interpreted cautiously, since EDS is a local and semi-quantitative technique and may reflect differences in the analyzed area, local redistribution of Cu-rich domains, or partial exposure of the inorganic phase after removal of superficial organic material. Overall, the combined gravimetric and microscopic results indicate that laundering does not appear to cause extensive detachment of the hybrid finish, although minor surface reorganization of the outermost coating layer cannot be excluded.

Infrared spectra collected in the cellulose-fingerprint region (1500–655 cm^{-1}) corroborate the microscopic observations (Fig. S1 in the Supplementary Material). For the neat GPTMS–TEOS finish (panel

a), the spectral envelope recorded after one and three laundering cycles exactly overlaps that of the unwashed sample, indicating that the siloxane network remains chemically intact. The same spectral stability is observed for the 2.04 wt% (panel b) and 4.08 wt% (panel c) CuI–PVA formulations: the intense Si–O–Si band at ~1030 cm^{-1}, the C–O–C cellulose peak at 1093 cm^{-1} and the C–H deformation modes at 1370–1460 cm^{-1} retain both position and intensity. Any solubilization of the coating would have produced a relative increase in cellulose absorption or the emergence of detergent-related bands, neither of which is observed. The FTIR data therefore support the persistence of the hybrid layer under the tested laundering conditions, although they do not provide a quantitative measure of coating loss.

The microbiological results mirror the physicochemical durability. As reported in Table 1, the untreated cotton and inert siloxane–coated cotton exhibit no biocidal activity. Conversely, the CuI–PVA coatings achieve a reduction of more than 99% in both pathogens. Crucially, this antimicrobial performance is retained after laundering. Indeed, the 2.04 wt% fabric suppressed 100.0% ± 0.0% of *S. aureus* cells and 99.5% ± 0.02% of *E. coli* cells after three wash cycles, whereas the 4.08 wt% fabric maintained complete (100.0% ± 0.0%) suppression of *S. aureus* and 98.7% ± 1.84% reduction of *E. coli*. The marginal drop against Gram-negative bacteria at the highest wash number is well within the statistical uncertainty and does not compromise hygienic performance.

These results show that the hybrid GPTMS–TEOS CuI–PVA coating retains marked antibacterial activity after three ISO 105-C10 washing cycles. Together with the gravimetric, SEM-EDS, and FTIR observations, the microbiological data support coating persistence and functional retention under the limited laundering protocol tested here. However, extended laundering, quantitative coating-loss assessment, copper-release monitoring, and post-aging antibacterial testing are required before long-term durability for repeated-use textile applications can be established.

3.7. Color assessment

Table 3 presents the color-space coordinates, expressed in the CIE L*a*b* system, of untreated and treated cotton samples. The untreated fabric exhibits a lightness (L*) value of 94.94, with a* and b* values of −0.76 and 2.12, respectively, indicating a predominantly white hue with high lightness. Applying the inorganic sol–gel layer (CO_GT) resulted in only a slight chromatic shift ($\Delta E^* = 0.20 \pm 0.01$) and a minor 3% reduction in W_{CIE}. This was primarily due to the subtle translucence and faint yellow tint typically associated with polysiloxane networks formed under acidic conditions. As ΔE^* remained below one, the perceptibility threshold defined by the CMC system, the sol–gel treatment is considered visually unobtrusive. In contrast, incorporating CuI–PVA particles significantly altered the optical appearance of the fabric. At a loading of 2.04 wt%, the treated fabric (CO_GT CuI–PVA-2%) showed a noticeable color difference ($\Delta E^* = 1.59 \pm 0.00$) and a 13% decrease in whiteness. Meanwhile, the 4.08 wt% formulation intensified both effects ($\Delta E^* = 2.09 \pm 0.01$; $W_{CIE} = 58.8$). The simultaneous shift of a* toward more negative values and the increase of b* toward higher positive values indicate a greenish-yellow hue, which is consistent with the broad visible absorption associated with Cu(I) stabilized by the PVA matrix. Laundering had different effects on the two finishing routes. For the neat sol–gel system, one domestic wash cycle was sufficient to restore the whiteness index to the level of the untreated fabric ($W_{CIE} \approx 72.4$) and lower ΔE^* to below 0.12. After three cycles, the W_{CIE} slightly exceeded the control level (73.4) and the ΔE^* remained imperceptible (0.23), suggesting that the siloxane-rich framework was largely retained while loosely bound oligomeric species were removed.

In contrast, the CuI–PVA finishes maintained their distinctive hue during laundering. The 2.04 wt% sample exhibited only a slight additional color change after one and three cycles ($\Delta E^* = 0.49$ and 0.91, respectively), whereas the 4.08 wt% specimen approached the unit threshold after the third wash ($\Delta E^* = 1.12$). Whiteness values varied within experimental error, but remained roughly constant (approximately 62 ± 1 for both concentrations), confirming that the functional particulate phase was strongly retained. The increase in ΔE^* remained below one unit per laundering cycle, demonstrating acceptable shade stability for functional textiles. These results indicate that the undoped sol–gel finish remains visually neutral under the tested washing conditions, whereas the CuI–PVA formulations intentionally shift the shade toward a yellowish-green hue associated with the copper-containing phase. After 1 and 3 ISO 105-C10 washing cycles, only limited additional color changes were observed. These colorimetric data therefore describe wash-related optical stability under the tested laundering protocol and should not be interpreted as evidence of photo-oxidative stability under real-use light/oxygen exposure.

Table 3
CIE L*a*b* coordinates (mean ± SD, n = 5), color difference ΔE^* (vs. untreated), and CIE whiteness index (W_{CIE}, D65/10°) for cotton fabrics: untreated (CO_UT), sol–gel finished (CO_GT), sol–gel-based CuI–PVA at 2.04 wt% and 4.08 wt% (CO_GT CuI–PVA 2% and CO_GT CuI–PVA 4%, respectively) before and after 1, and 3 washes. (The reference sample for W_{CIE} is always CO_UT; the reference for CIE L*a*b* are CO_UT, CO_GT, CO_GT CuI–PVA 2%, CO_GT CuI–PVA 4% for treated samples, sol–gel treated samples, GT CuI–PVA 2% treated samples, and GT CuI–PVA 4%, respectively).

Sample	L*	a*	b*	ΔE^*	W_{CIE}
CO_UT	94.94	−0.76	2.12		72.86 ± 0.189
CO_GT	94.83	−0.81	2.29	0.20 ± 0.011	70.76 ± 0.174
CO_GT CuI–PVA 2%	94.39	−1.28	3.52	1.59 ± 0.003	63.30 ± 0.341
CO_GT CuI–PVA 4%	94.15	−1.34	3.97	2.09 ± 0.008	58.80 ± 0.159
CO_GT	94.58	−0.76	2.33		70.76 ± 0.174
CO_GT 1W	94.64	−0.77	2.23	0.11 ± 0.019	72.43 ± 0.362
CO_GT 3W	94.66	−0.72	2.11	0.23 ± 0.021	73.43 ± 0.219
CO_GT CuI–PVA 2%	94.39	−1.28	3.52		63.30 ± 0.341
CO_GT CuI–PVA 2% 1W	94.23	−1.68	3.28	0.49 ± 0.015	63.44 ± 0.307
CO_GT CuI–PVA 2% 3W	94.06	−2.10	3.29	0.91 ± 0.026	62.60 ± 0.446
CO_GT CuI–PVA 4%	94.15	−1.34	3.97		58.80 ± 0.159
CO_GT CuI–PVA 4% 1W	94.13	−1.81	3.56	0.62 ± 0.019	62.26 ± 0.533
CO_GT CuI–PVA 4% 3W	93.86	−2.31	3.49	1.12 ± 0.011	61.51 ± 0.697

4. Conclusion

This study presents a proof-of-concept CuI–PVA/siloxane sol–gel finishing for imparting antibacterial functionality to cotton fabrics through a conventional pad–dry–cure process. The spectroscopic and microscopic analyses supported the formation of a hybrid coating containing a CuI–PVA phase within a GPTMS–TEOS-derived siloxane matrix, while SEM-EDS and FTIR observations after washing indicated persistence of the coating under the tested laundering conditions. Both CuI–PVA-containing formulations showed marked antibacterial activity against *S. aureus* and *E. coli* under the tested conditions, and this activity was substantially retained after three ISO 105-C10 washing cycles. Bending stiffness measurements showed only a limited increase after finishing, suggesting no marked stiffening under the conditions investigated.

The present results support the proposed system as a simple and scalable proof-of-concept antibacterial finish for cotton. However, the study does not establish long-term durability or full textile performance. Extended laundering, including higher numbers of washing cycles,

quantitative coating-loss and copper-release analyses, tensile and abrasion testing, air and water-vapor permeability measurements, cytotoxicity/skin-compatibility assays, photo-aging studies, ROS-specific mechanistic tests, XPS, and XRD characterization are required before practical deployment in medical or consumer textile applications can be fully validated.

CRediT authorship contribution statement

Valentina Trovato: Writing – review & editing, Writing – original draft, Visualization, Validation, Methodology, Investigation, Data curation, Conceptualization. **Maria Josè Lo Faro:** Writing – review & editing, Writing – original draft, Visualization, Validation, Investigation, Data curation. **Giulia Rando:** Writing – review & editing, Writing – original draft, Visualization, Validation, Data curation. **Maurilio Galletta:** Writing – original draft, Validation, Methodology, Investigation, Data curation, Conceptualization. **Agnese D'Agostino:** Writing – original draft, Investigation, Formal analysis, Data curation. **Serena Facchiano:** Writing – original draft, Validation, Investigation, Formal analysis, Data curation. **Claudia Vineis:** Writing – review & editing, Visualization, Validation, Resources, Methodology. **Raphael Palucci Rosa:** Writing – review & editing, Writing – original draft, Visualization, Validation, Investigation, Data curation. **Silvia Sfameni:** Writing – original draft, Visualization, Validation, Formal analysis. **Giuseppe Rosace:** Writing – review & editing, Writing – original draft, Visualization, Validation, Supervision, Resources, Project administration, Methodology, Conceptualization. **Maria Rosaria Plutino:** Writing – review & editing, Writing – original draft, Visualization, Validation, Supervision, Resources, Methodology, Conceptualization.

Declaration of competing interest

The authors declare that they have no known competing financial interests or personal relationships that could have appeared to influence the work reported in this paper.

Acknowledgements

This study was carried out within the MICS (Made in Italy Circular and Sustainable) Extended Partnership and received funding from the European Union Next-Generation EU (Piano Nazionale Di Ripresa E Resilienza (PNRR)—Missione 4 Componente 2, Investimento 1.3—D.D. 1551.11-10-2022, PE00000004), and the I-PHOQS project funded by the European Union (NextGeneration EU) through the MUR-PNRR (CUP: B53C22001750006). This manuscript reflects only the authors' views and opinions, neither the European Union nor the European Commission can be considered responsible for them.

The authors acknowledge Dr. Mariam Hadhri (Department of Engineering and Applied Sciences, University of Bergamo) for Datacolor analysis.

Supplementary materials

Supplementary material associated with this article can be found, in the online version, at doi:10.1016/j.surfin.2026.110232.

Data availability

Data will be made available on request.

References

[1] U. Abdul-Reda Hussein, Z.H. Mahmoud, K.M.A. Alaziz, M.L. Alid, Y. Yasin, F.K. Ali, A.N. Faisal, A.N. Abd, E. Kianfar, Antimicrobial finishing of textiles using nanomaterials, Brazilian Journal of Biology 84 (2024), https://doi.org/10.1590/1519-6984.264947.

[2] L.E. Román, E.D. Gomez, J.L. Solís, M.M. Gómez, Antibacterial Cotton Fabric Functionalized with Copper Oxide Nanoparticles, Molecules 25 (2020) 5802, https://doi.org/10.3390/molecules25245802.

[3] S.J. Dancer, Controlling Hospital-Acquired Infection: Focus on the Role of the Environment and New Technologies for Decontamination, Clin. Microbiol. Rev. 27 (2014) 665–690, https://doi.org/10.1128/CMR.00020-14.

[4] H. Morris, R. Murray, Medical Textiles, CRC Press, Boca Raton, 2021, https://doi.org/10.1201/9781003170570.

[5] Md.R. Repon, T. Islam, H.T. Sadia, D. Mikučionienė, S. Hossain, G. Kibria, M. Kaseem, Development of Antimicrobial Cotton Fabric Impregnating AgNPs Utilizing Contemporary Practice, Coatings 11 (2021) 1413, https://doi.org/10.3390/coatings11111413.

[6] M. Karypidis, E. Karanikas, A. Papadaki, E.G. Andriotis, A Mini-Review of Synthetic Organic and Nanoparticle Antimicrobial Agents for Coatings in Textile Applications, Coatings 13 (2023) 693, https://doi.org/10.3390/coatings13040693.

[7] D. Morais, R. Guedes, M. Lopes, Antimicrobial Approaches for Textiles: From Research to Market, Materials 9 (2016) 498, https://doi.org/10.3390/ma9060498.

[8] F. Tanasa, C.-A. Teaca, M. Nechifor, M. Ignat, I.A. Duceac, L. Ignat, Highly Specialized Textiles with Antimicrobial Functionality—Advances and Challenges, Textiles 3 (2023) 219–245, https://doi.org/10.3390/textiles3020015.

[9] N. Agrawal, P.S. Low, J.S.J. Tan, E.W.M. Fong, Y. Lai, Z. Chen, Durable easy-cleaning and antibacterial cotton fabrics using fluorine-free silane coupling agents and CuO nanoparticles, Nano Materials Science 2 (2020) 281–291, https://doi.org/10.1016/j.nanoms.2019.09.004.

[10] M. Radetić, D. Marković, Nano-finishing of cellulose textile materials with copper and copper oxide nanoparticles, Cellulose 26 (2019) 8971–8991, https://doi.org/10.1007/s10570-019-02714-4.

[11] D. Chen, Z. Mai, X. Liu, D. Ye, H. Zhang, X. Yin, Y. Zhou, M. Liu, W. Xu, UV-blocking, superhydrophobic and robust cotton fabrics fabricated using polyvinylsilsesquioxane and nano-TiO2, Cellulose 25 (2018) 3635–3647, https://doi.org/10.1007/s10570-018-1790-7.

[12] S. Ortelli, M. Vespignani, I. Zanoni, M. Blosi, C. Vineis, A. Piancastelli, G. Baldi, V. Dami, S. Albonetti, A. Costa, Design of TiO2-Based Hybrid Systems with Multifunctional Properties, Molecules 28 (2023) 1863, https://doi.org/10.3390/molecules28041863.

[13] M. Salas-Orozco, N. Niño-Martínez, G.-A. Martínez-Castañón, F.T. Méndez, M.E. C. Jasso, F. Ruiz, Mechanisms of Resistance to Silver Nanoparticles in Endodontic Bacteria: A Literature Review, J. Nanomater. 2019 (2019) 1–11, https://doi.org/10.1155/2019/7630316.

[14] A. Panáček, L. Kvítek, M. Smékalová, R. Večeřová, M. Kolář, M. Röderová, F. Dyčka, M. Šebela, R. Prucek, O. Tomanec, R. Zbořil, Bacterial resistance to silver nanoparticles and how to overcome it, Nat. Nanotechnol. 13 (2018) 65–71, https://doi.org/10.1038/s41565-017-0013-y.

[15] G. Dhillon, S. Kaur, R. Pulicharla, S. Brar, M. Cledón, M. Verma, R. Surampalli, Triclosan: Current Status, Occurrence, Environmental Risks and Bioaccumulation Potential, Int. J. Environ. Res. Public Health 12 (2015) 5657–5684, https://doi.org/10.3390/ijerph120505657.

[16] E. Lombi, E. Donner, K.G. Scheckel, R. Sekine, C. Lorenz, N. Von Goetz, B. Nowack, Silver speciation and release in commercial antimicrobial textiles as influenced by washing, Chemosphere 111 (2014) 352–358, https://doi.org/10.1016/j.chemosphere.2014.03.116.

[17] D.M. Mitrano, E. Lombi, Y.A.R. Dasilva, B. Nowack, Unraveling the Complexity in the Aging of Nanoenhanced Textiles: A Comprehensive Sequential Study on the Effects of Sunlight and Washing on Silver Nanoparticles, Environ. Sci. Technol. 50 (2016) 5790–5799, https://doi.org/10.1021/acs.est.6b01478.

[18] R. Arvidsson, S. Molander, B.A. Sandén, Impacts of a Silver-Coated Future, J. Ind. Ecol. 15 (2011) 844–854, https://doi.org/10.1111/j.1530-9290.2011.00400.x.

[19] K.M. Archana, R. Rajagopal, V.G. Krishnaswamy, S. Aishwarya, Application of green synthesised copper iodide particles on cotton fabric-protective face mask material against COVID-19 pandemic, Journal of Materials Research and Technology 15 (2021) 2102–2116, https://doi.org/10.1016/j.jmrt.2021.09.020.

[20] V. Molahalli, A. Sharma, K. Bijapur, G. Soman, A. Shetty, B. Sirichandana, B.G.M. Patel, N. Chattham, G. Hegde, Properties, Synthesis, and Characterization of Cu-Based Nanomaterials, in: 2024: pp. 1–33. https://doi.org/10.1021/bk-2024-1466.ch001.

[21] A. Pramanik, D. Laha, D. Bhattacharya, P. Pramanik, P. Karmakar, A novel study of antibacterial activity of copper iodide nanoparticle mediated by DNA and membrane damage, Colloids Surf. B Biointerfaces 96 (2012) 50–55, https://doi.org/10.1016/j.colsurfb.2012.03.021.

[22] L. Wang, C. Hu, L. Shao, The antimicrobial activity of nanoparticles: present situation and prospects for the future, Int. J. Nanomedicine Volume 12 (2017) 1227–1249, https://doi.org/10.2147/IJN.S121956.

[23] G. Mary, S.K. Bajpai, N. Chand, Copper (II) ions and copper nanoparticles-loaded chemically modified cotton cellulose fibers with fair antibacterial properties, J. Appl. Polym. Sci. 113 (2009) 757–766, https://doi.org/10.1002/app.29890.

[24] I.M. El-Nahhal, S.M. Zourab, F.S. Kodeh, M. Selmane, I. Genois, F. Babonneau, Nanostructured copper oxide-cotton fibers: synthesis, characterization, and applications, Int, Nano Lett 2 (2012) 14, https://doi.org/10.1186/2228-5326-2-14.

[25] S. Adewale Akintelu, A. Kolawole Oyebamiji, S. Charles Olugbeko, D. Felix Latona, Green chemistry approach towards the synthesis of copper nanoparticles and its potential applications as therapeutic agents and environmental control, Current Research in Green and Sustainable Chemistry 4 (2021) 100176, https://doi.org/10.1016/j.crgsc.2021.100176.

[26] R. Betancourt-Galindo, P.Y. Reyes-Rodriguez, B.A. Puente-Urbina, C.A. Avila-Orta, O.S. Rodríguez-Fernández, G. Cadenas-Pliego, R.H. Lira-Saldivar, L.A. García-Cerda, Synthesis of Copper Nanoparticles by Thermal Decomposition and Their Antimicrobial Properties, J. Nanomater. 2014 (2014), https://doi.org/10.1155/2014/980545.
[27] K. Dobrovolný, P. Ulbrich, M. Švecová, V. Bartůněk, Affordable, Green, and Facile Synthesis of Copper Nanoparticles Stabilized by Environmentally Friendly Surfactants, Metallurgical and Materials Transactions B 46 (2015) 2529–2533, https://doi.org/10.1007/s11663-015-0424-9.
[28] H. Lee, S.H. Park, S.-G. Seo, S.-J. Kim, S.-C. Kim, Y.-K. Park, S.-C. Jung, Preparation and Characterization of Copper Nanoparticles via the Liquid Phase Plasma Method, Curr. Nanosci. 10 (2014) 7–10, https://doi.org/10.2174/15734137096661311112217 41.
[29] B. Wang, S. Chen, J. Nie, X. Zhu, Facile method for preparation of superfine copper nanoparticles with high concentration of copper chloride through photoreduction, RSC Adv 4 (2014) 27381–27388, https://doi.org/10.1039/C4RA02870H.
[30] J.N. Solanki, R. Sengupta, Z.V.P. Murthy, Synthesis of copper sulphide and copper nanoparticles with microemulsion method, Solid State Sci 12 (2010) 1560–1566, https://doi.org/10.1016/j.solidstatesciences.2010.06.021.
[31] S. Yallappa, J. Manjanna, M.A. Sindhe, N.D. Satyanarayan, S.N. Pramod, K. Nagaraja, Microwave assisted rapid synthesis and biological evaluation of stable copper nanoparticles using T. arjuna bark extract, Spectrochim. Acta A Mol. Biomol. Spectrosc. 110 (2013) 108–115, https://doi.org/10.1016/j.saa.2013.03.005.
[32] M. Saito, K. Yasukawa, T. Umeda, Y. Aoi, Copper nanoparticles fabricated by laser ablation in polysiloxane, Opt. Mater. (Amst). 30 (2008) 1201–1204, https://doi.org/10.1016/j.optmat.2007.05.049.
[33] I. Perelshtein, G. Applerot, N. Perkas, E. Wehrschuetz-Sigl, A. Hasmann, G. Guebitz, A. Gedanken, CuO–cotton nanocomposite: Formation, morphology, and antibacterial activity, Surface and Coatings Technology 204 (2009) 54–57, https://doi.org/10.1016/j.surfcoat.2009.06.028.
[34] A. Bashiri Rezaie, M. Montazer, M. Mahmoudi Rad, Environmentally friendly low cost approach for nano copper oxide functionalization of cotton designed for antibacterial and photocatalytic applications, Journal of Cleaner Production 204 (2018) 425–436, https://doi.org/10.1016/j.jclepro.2018.08.337.
[35] N. Zhu, S. Zhou, J. Gong, X. Wang, C. Zhang, W. Li, D. Sheng, X. Liu, L. Xia, W. Xu, In situ synthesis of cuprous oxide on cotton fiber for developing functional textile with broad-spectrum antibacterial activity, Industrial Crops and Products 187 (2022) 115442, https://doi.org/10.1016/j.indcrop.2022.115442.
[36] A.X. Chen, D.K.R. Beins, Y. Wang, H.-K. Luo, Y.Y. Yang, N. Li, Fast-Acting and Skin-Compatible Antimicrobial Coating on Cotton Fabrics via In Situ Self-Assembly of Phosphine-Coordinated Copper Iodide Clusters, ACS Applied Engineering Materials 2 (2024) 2864–2874, https://doi.org/10.1021/acsaenm.4c00548.
[37] J.M.I.Sonali Mughilmathi, P.S. Kumar, K.M. Archana, R. Rajagopal, K.V. Gayathri, Application of copper iodide (CuI) and natural dye extracted from Hibiscus rosa-sinensis onto cotton fabric: an integrated approach, Applied Nanoscience 13 (2023) 4119–4128, https://doi.org/10.1007/s13204-022-02720-2.
[38] M. Avatefi Hemmat, S. Asghari, M. Bakhshesh, M. Mahmoudifard, Copper iodide decorated graphene oxide as a highly efficient antibacterial and antiviral nanocomposite, Inorg. Chem. Commun. 156 (2023) 111214, https://doi.org/10.1016/j.inoche.2023.111214.
[39] D. Chen, Y. Wang, Z. Lin, J. Huang, X. Chen, D. Pan, F. Huang, Growth Strategy and Physical Properties of the High Mobility P-Type CuI Crystal, Cryst. Growth Des. 10 (2010) 2057–2060, https://doi.org/10.1021/cg100270d.
[40] S.L. Dhere, S.S. Latthe, C. Kappenstein, S.K. Mukherjee, A.V. Rao, Comparative studies on p-type CuI grown on glass and copper substrate by SILAR method, Appl. Surf. Sci. 256 (2010) 3967–3971, https://doi.org/10.1016/j.apsusc.2010.01.058.
[41] Y. Zhou, M. Lü, G. Zhou, S. Wang, S. Wang, Preparation and photoluminescence of γ-CuI nanoparticles, Mater. Lett. 60 (2006) 2184–2186, https://doi.org/10.1016/j.matlet.2005.12.093.
[42] X. Hu, J.C. Yu, J. Gong, Q. Li, A Facile Surface-Etching Route to Thin Films of Metal Iodides, Cryst. Growth Des. 7 (2007) 262–267, https://doi.org/10.1021/cg060288p.
[43] X. Li, M. Wan, Morphology and Hydrophobicity of Micro/Nanoscaled Cuprous Iodide Crystal, Cryst. Growth Des. 6 (2006) 2661–2666, https://doi.org/10.1021/cg050644o.
[44] S. Alven, S. Peter, Z. Mbese, B.A. Aderibigbe, Polymer-Based Wound Dressing Materials Loaded with Bioactive Agents: Potential Materials for the Treatment of Diabetic Wounds, Polymers (Basel) 14 (2022) 724, https://doi.org/10.3390/polym14040724.
[45] B. Turakhia, M.B. Divakara, M.S. Santosh, S. Shah, Green synthesis of copper oxide nanoparticles: a promising approach in the development of antibacterial textiles, J. Coat. Technol. Res. 17 (2020) 531–540, https://doi.org/10.1007/s11998-019-00303-5.
[46] G. Pal, P. Rai, A. Pandey, Green synthesis of nanoparticles: A greener approach for a cleaner future, in: Green Synthesis, Characterization and Applications of Nanoparticles, Elsevier (2019) 1–26, https://doi.org/10.1016/B978-0-08-102579-6.00001-0.
[47] S. Inkinen, M. Hakkarainen, A.-C. Albertsson, A. Södergård, From Lactic Acid to Poly(lactic acid) (PLA): Characterization and Analysis of PLA and Its Precursors, Biomacromolecules 12 (2011) 523–532, https://doi.org/10.1021/bm101302t.
[48] A. Sinha, S.K. Das, V. Rao, P. Ramachandrarao, Patterning of copper particles on polymeric surface, J. Mater. Res. 16 (2001) 1354–1357, https://doi.org/10.1557/JMR.2001.0189.
[49] K. Dobrovolný, P. Ulbrich, M. Švecová, S. Rimpelová, J. Malinčík, M. Kohout, J. Svoboda, V. Bartůněk, Copper nanoparticles in glycerol-polyvinyl alcohol matrix: In situ preparation, stabilisation and antimicrobial activity, J. Alloys Compd. 697 (2017) 147–155, https://doi.org/10.1016/j.jallcom.2016.12.144.
[50] A.Reza Hajipour, F. Mohammadsaleh, M.Reza Sabzalian, Copper-containing polyvinyl alcohol composite systems: Preparation, characterization and biological activity, Journal of Physics and Chemistry of Solids 83 (2015) 96–103, https://doi.org/10.1016/j.jpcs.2015.03.010.
[51] B. Mahltig, T. Textor, Nanosols and Textiles, WORLD SCIENTIFIC, 2008. https://doi.org/10.1142/6961.
[52] F. Puoci, C. Saturnino, V. Trovato, D. Iacopetta, E. Piperopoulos, C. Triolo, M. G. Bonomo, D. Drommi, O.I. Parisi, C. Milone, M.S. Sinicropi, G. Rosace, M. R. Plutino, Sol–Gel Treatment of Textiles for the Entrapping of an Antioxidant/Anti-Inflammatory Molecule: Functional Coating Morphological Characterization and Drug Release Evaluation, Applied Sciences 10 (2020) 2287, https://doi.org/10.3390/app10072287.
[53] N.N. Khimich, Synthesis of Silica Gels and Organic-Inorganic Hybrids on Their Base, Glass Physics and Chemistry 30 (2004) 430–442, https://doi.org/10.1023/B:GPAC.0000045925.84139.eb.
[54] V. Trovato, E. Teblum, Y. Kostikov, A. Pedrana, V. Re, G.D. Nessim, G. Rosace, Sol-gel approach to incorporate millimeter-long carbon nanotubes into fabrics for the development of electrical-conductive textiles, Mater. Chem. Phys. 240 (2020) 122218, https://doi.org/10.1016/j.matchemphys.2019.122218.
[55] C. Colleoni, M.R. Massafra, G. Rosace, Photocatalytic properties and optical characterization of cotton fabric coated via sol–gel with non-crystalline TiO2 modified with poly(ethylene glycol), Surf. Coat. Technol. 207 (2012) 79–88, https://doi.org/10.1016/j.surfcoat.2012.06.003.
[56] S. Sfameni, T. Lawnick, G. Rando, A. Visco, T. Textor, M.R. Plutino, Functional Silane-Based Nanohybrid Materials for the Development of Hydrophobic and Water-Based Stain Resistant Cotton Fabrics Coatings, Nanomaterials 12 (2022) 3404, https://doi.org/10.3390/nano12193404.
[57] V. Trovato, S. Sfameni, R. Ben Debabis, G. Rando, G. Rosace, G. Malucelli, M. R. Plutino, How to Address Flame-Retardant Technology on Cotton Fabrics by Using Functional Inorganic Sol–Gel Precursors and Nanofillers: Flammability Insights, Research Advances, and Sustainability Challenges, Inorganics (Basel) 11 (2023) 306, https://doi.org/10.3390/inorganics11070306.
[58] V. Trovato, G. Iacono, G. Malucelli, G. Rosace, Silica-Containing Phosphorus-Based Sol-Gel Finishing to Improve Flame Retardant Performance of Cotton Fabrics, Materials Science Forum 1117 (2024) 23–28, https://doi.org/10.4028/p-usqR8L.
[59] S. Sfameni, G. Rando, M.R. Plutino, Sustainable Secondary-Raw Materials, Natural Substances and Eco-Friendly Nanomaterial-Based Approaches for Improved Surface Performances: An Overview of What They Are and How They Work, Int. J. Mol. Sci. 24 (2023), https://doi.org/10.3390/ijms24065472.
[60] S. Sfameni, T. Lawnick, G. Rando, A. Visco, T. Textor, M.R. Plutino, Super-Hydrophobicity of Polyester Fabrics Driven by Functional Sustainable Fluorine-Free Silane-Based Coatings, Gels 9 (2023) 109, https://doi.org/10.3390/gels9020109.
[61] R.R. Bhosale, R.V. Shende, J.A. Puszynski, Thermochemical water-splitting for H2 generation using sol-gel derived Mn-ferrite in a packed bed reactor, Int. J. Hydrogen Energy 37 (2012) 2924–2934, https://doi.org/10.1016/j.ijhydene.2011.03.010.
[62] V. Trovato, A. Mezzi, M. Brucale, H. Abdeh, D. Drommi, G. Rosace, M.R. Plutino, Sol-Gel Assisted Immobilization of Alizarin Red S on Polyester Fabrics for Developing Stimuli-Responsive Wearable Sensors, Polymers (Basel) 14 (2022) 2788, https://doi.org/10.3390/polym14142788.
[63] G. Rando, E. Scalone, S. Sfameni, M.R. Plutino, Functional Bio-Based Polymeric Hydrogels for Wastewater Treatment: From Remediation to Sensing Applications, Gels 10 (2024) 498, https://doi.org/10.3390/gels10080498.
[64] Z. Liu, Z. Ma, B. Qian, A.Y.H. Chan, X. Wang, Y. Liu, J.H. Xin, A Facile and Scalable Method of Fabrication of Large-Area Ultrathin Graphene Oxide Nanofiltration Membrane, ACS Nano 15 (2021) 15294–15305, https://doi.org/10.1021/acsnano.1c06155.
[65] T.A. Elmaaty, S. Raouf, K. Sayed-Ahmed, M.R. Plutino, Multifunctional Dyeing of Wool Fabrics Using Selenium Nanoparticles, Polymers (Basel) 14 (2022) 191, https://doi.org/10.3390/polym14010191.
[66] G. Rando, S. Sfameni, M. Hadhri, A. Mezzi, M. Brucale, G. De Luca, E. Piperopoulos, C. Milone, D. Drommi, G. Rosace, V. Trovato, M.R. Plutino, Methyl Red-loaded halloysite nanotubes-based silica coatings for durable dyeing of polyester fabrics, Surfaces and Interfaces 53 (2024) 105006, https://doi.org/10.1016/j.surfin.2024.105006.
[67] M. Hadhri, C. Colleoni, A. D'Agostino, M. Erhaim, R.P. Rosa, G. Rosace, V. Trovato, Eco-Friendly Octylsilane-Modified Amino-Functional Silicone Coatings for a Durable Hybrid Organic–Inorganic Water-Repellent Textile Finish, Polymers (Basel) 17 (2025) 1578, https://doi.org/10.3390/polym17111578.
[68] C. Sanchez, G.J.D.A.A. Soler-Illia, F. Ribot, D. Grosso, Design of functional nano-structured materials through the use of controlled hybrid organic–inorganic interfaces, Comptes Rendus. Chimie 6 (2003) 1131–1151, https://doi.org/10.1016/j.crci.2003.06.001.
[69] D.A. Monteiro, G. Gozzi, D.L. Chinaglia, O.N. Oliveira, F.S. de Vicente, Proton conduction mechanisms in GPTMS/TEOS-derived organic/silica hybrid films prepared by sol-gel process, Synthetic Metals 267 (2020) 116448, https://doi.org/10.1016/j.synthmet.2020.116448.
[70] F.X. Perrin, F. Ziarelli, A. Dupuis, Relation between the corrosion resistance and the chemical structure of hybrid sol-gel coatings with interlinked inorganic-organic network, Progress in Organic Coatings 141 (2020) 105532, https://doi.org/10.1016/j.porgcoat.2019.105532.

[71] ISO 105-J02:1997 - Textiles — Tests for colour fastness — Part J02: Instrumental assessment of relative whiteness, International Organization for Standardization, 1997.
[72] ISO 105-J03:2009; Textiles—Tests for Colour Fastness Part J03: Calculation of Colour Differences, International Organization for Standardization, 2009.
[73] ASTM International. Standard Test Method for Determining the Antimicrobial Activity of Antimicrobial Agents Under Dynamic Contact Conditions, ASTM, 2025, pp. E2149–25, https://doi.org/10.1520/E2149-25.
[74] DIN 53362:2024-11; Coated or Not Coated Plastics—Determination of Stiffness in Bending Method According to Cantilever, German Institute for Standardisation (Deutsches Institut für Normung), Berlin, Germany, 2024 n.d.
[75] V. Trovato, R. Konar, E. Teblum, P. Lazzaroni, V. Re, G. Rosace, G.D. Nessim, Humidity- and Temperature-Sensing Properties of 2D-Layered Tungsten Di-Selenide (2H-WSe2) Electroconductive Coatings for Cotton-Based Smart Textiles, Polymers (Basel) 17 (2025) 752, https://doi.org/10.3390/polym17060752.
[76] V. Trovato, A. Mezzi, M. Brucale, G. Rosace, M.Rosaria Plutino, Alizarin-functionalized organic-inorganic silane coatings for the development of wearable textile sensors, J. Colloid Interface Sci. 617 (2022) 463–477, https://doi.org/10.1016/j.jcis.2022.03.006.
[77] P. Phetcharat, P. Sangsanoh, C. Choipang, S. Chaiarwut, O. Suwantong, P. Chuysinuan, P. Supaphol, Curative Effects of Copper Iodide Embedded on Gallic Acid Incorporated in a Poly(vinyl alcohol) (PVA) Liquid Bandage, Gels 9 (2023) 53, https://doi.org/10.3390/gels9010053.
[78] K. Nakamoto, Infrared and Raman Spectra of Inorganic and Coordination Compounds, Wiley, 2008, https://doi.org/10.1002/9780470405840.
[79] H.R. Lucas, G.J. Meyer, K.D. Karlin, CO and O 2 Binding to Pseudo-tetradentate Ligand−Copper(I) Complexes with a Variable N-Donor Moiety: Kinetic/Thermodynamic Investigation Reveals Ligand-Induced Changes in Reaction Mechanism, J. Am. Chem. Soc. 132 (2010) 12927–12940, https://doi.org/10.1021/ja104107q.
[80] A. Alessi, S. Agnello, G. Buscarino, F.M. Gelardi, Raman and IR investigation of silica nanoparticles structure, J. Non. Cryst. Solids 362 (2013) 20–24, https://doi.org/10.1016/j.jnoncrysol.2012.11.006.
[81] A. Bertoluzza, C. Fagnano, M. Antonietta Morelli, V. Gottardi, M. Guglielmi, Raman and infrared spectra on silica gel evolving toward glass, J. Non. Cryst. Solids 48 (1982) 117–128, https://doi.org/10.1016/0022-3093(82)90250-2.
[82] L. de Ferri, P.P. Lottici, A. Lorenzi, A. Montenero, E. Salvioli-Mariani, Study of silica nanoparticles – polysiloxane hydrophobic treatments for stone-based monument protection, J. Cult. Herit. 12 (2011) 356–363, https://doi.org/10.1016/j.culher.2011.02.006.
[83] I.M. Šapić, L. Bistričić, V. Volovšek, V. Dananić, K. Furić, DFT study of molecular structure and vibrations of 3-glycidoxypropyltrimethoxysilane, Spectrochim. Acta A Mol. Biomol. Spectrosc. 72 (2009) 833–840, https://doi.org/10.1016/j.saa.2008.11.032.
[84] S.F. Soares, T. Trindade, A.L. Daniel-da-Silva, Enhanced Removal of Non-Steroidal Inflammatory Drugs from Water by Quaternary Chitosan-Based Magnetic Nanosorbents, Coatings 11 (2021) 964, https://doi.org/10.3390/coatings11080964.
[85] Y. Kawano, S. Denofre, Y. Gushikem, Raman and infrared spectra of silica gel and niobium(V) oxide grafted on silica gel surface and their dependence on pretreatment temperatures, Vib. Spectrosc. 7 (1994) 293–302, https://doi.org/10.1016/0924-2031(94)85019-4.
[86] D.K. Kaushik, M. Selvaraj, S. Ramu, A. Subrahmanyam, Thermal evaporated Copper Iodide (CuI) thin films: A note on the disorder evaluated through the temperature dependent electrical properties, Solar Energy Materials and Solar Cells 165 (2017) 52–58, https://doi.org/10.1016/j.solmat.2017.02.030.
[87] M. Sadat-Shojai, M.-T. Khorasani, E. Dinpanah-Khoshdargi, A. Jamshidi, Synthesis methods for nanosized hydroxyapatite with diverse structures, Acta Biomaterialia 9 (2013) 7591–7621, https://doi.org/10.1016/j.actbio.2013.04.012.
[88] C. Schramm, B. Rinderer, Non-formaldehyde, crease-resistant modification of cellulosic material by means of an organotrialkoxysilane and metal alkoxides, Cellulose 22 (2015) 2811–2824, https://doi.org/10.1007/s10570-015-0664-5.
[89] A. Bacciarelli-Ulacha, E. Matyjas-Zgondek, D. Puchowicz, M. Cieslak, Comparison of Innovative Silver Nanoparticles Finishing Technologies to Obtain Antibacterial Properties of Cotton Fabric, Fibers and Polymers 23 (2022) 2606–2615, https://doi.org/10.1007/s12221-022-4327-5.
[90] I.Yu. Prosanov, V.A. Volodin, Raman scattering behavior of hybrid polymeric complexes of polyvinyl alcohol with $CuCl_2$ and $Cu(OH)_2$/CuO, Physics of the Solid State 66 (2024) 968–972, https://doi.org/10.61011/PSS.2024.06.58712.116.
[91] L.B. Capeletti, I.M. Baibich, I.S. Butler, J.H.Z. dos Santos, Infrared and Raman spectroscopic characterization of some organic substituted hybrid silicas, Spectrochim. Acta A Mol. Biomol. Spectrosc. 133 (2014) 619–625, https://doi.org/10.1016/j.saa.2014.05.072.
[92] M.K. Eberhardt, G. Ramirez, E. Ayala, Does the reaction of copper(I) with hydrogen peroxide give hydroxyl radicals? A study of aromatic hydroxylation, J. Org. Chem. 54 (1989) 5922–5926, https://doi.org/10.1021/jo00286a024.
[93] A.X. Chen, H.Y. Lau, J.Y. Teo, Y. Wang, D.Z.Y. Choong, Y. Wang, H.-K. Luo, Y. Y. Yang, N. Li, Water-Mediated In, Situ Fabrication of CuI Nanoparticles on Flexible Cotton Fabrics as a Sustainable and Skin-Compatible Coating with Broad-Spectrum Antimicrobial Efficacy, ACS Applied Nano Materials 6 (2023) 13238–13249, https://doi.org/10.1021/acsanm.3c01961.
[94] R. Hernandez, A. Jimenez-Chávez, A. De Vizcaya, J.A. Lozano-Alvarez, K. Esquivel, I.E. Medina-Ramírez, Synthesis of TiO2-Cu2+/CuI Nanocomposites and Evaluation of Antifungal and Cytotoxic Activity, Nanomaterials 13 (2023) 1900, https://doi.org/10.3390/nano13131900.
[95] X. Ma, S. Zhou, X. Xu, Q. Du, Copper-containing nanoparticles: Mechanism of antimicrobial effect and application in dentistry-a narrative review, Frontiers in Surgery 9 (2022), https://doi.org/10.3389/fsurg.2022.905892.
[96] J. Ramos-Zúñiga, N. Bruna, J.M. Pérez-Donoso, Toxicity Mechanisms of Copper Nanoparticles and Copper Surfaces on Bacterial Cells and Viruses, International Journal of Molecular Sciences 24 (2023) 10503, https://doi.org/10.3390/ijms241310503.
[97] D. Laha, D. Bhattacharya, A. Pramanik, C.R. Santra, P. Pramanik, P. Karmakar, Evaluation of copper iodide and copper phosphate nanoparticles for their potential cytotoxic effect, Toxicology Research 1 (2012) 131, https://doi.org/10.1039/c2tx00009a.